Climate
of the Past
Discussions

Did the Bronze Age deforestation of Europe affect its climate? A regional climate-model study using pollen-based land-cover reconstructions

Gustav Strandberg[1,2], Jie Chen[2,3,4], Ralph Fyfe[5], Erik Kjellström[1,2], Johan Lindström[6], Anneli Poska[7],
5   Qiong Zhang[2,3], Marie-José Gaillard[8]

[1]Rossby Centre, Swedish Meteorological and Hydrological Institute, SMHI, Norrköping, SE-602 19, Sweden
[2] Bolin Centre for Climate Research, Stockholm University, Stockholm, SE-106 91, Sweden
[3] Department of Physical Geography, Stockholm University, Stockholm, SE-106 91, Sweden
[4] College of Atmospheric Sciences, Lanzhou University, Lanzhou, 730000, China
10   [5]School of Geography, Earth and Environmental Sciences, University of Plymouth, Plymouth, PL4 8AA, UK
[6] Centre for Mathematical Sciences, Lund University, SE-221 00 Lund, Sweden
[7] Department of Geology, Tallinn University of Technology, 19086 Tallinn, Estonia
[8] Department of Biology and Environmental Science, Linnaeus University, SE-39231 Kalmar, Sweden

15   *Correspondence to*: Gustav Strandberg (gustav.strandberg@smhi.se)

Abstract. This paper studies the impact of land use and land-cover change (LULCC) on the climate around 2 500 years ago (2.5 ka), a period of rapid transitions across the European landscape. One global climate model was used to force two regional climate models (RCMs). The RCMs used two land cover descriptions. The first was from a dynamical vegetation model representing potential land cover; the second a land cover description reconstructed from pollen data by statistical interpolation.
20   The two different land covers enable us to study the impact of land cover on climate conditions. Since the difference in landscape openness between potential and reconstructed land cover is mostly due to LULCC, this can be taken as a measure of early anthropogenic effects on climate. The use of two RCMs enables us to study how sensitive climate models can be to land-cover changes.

The results show that the simulated 2.5 ka climate was warmer than the simulated pre-industrial (PI) climate. The largest
25   differences are seen in northern Europe, where the 2.5 ka climate is 2-4 °C warmer than PI. In summer, the difference between the simulated 2.5 ka and PI climates is smaller (0-3 °C), with the smallest differences in southern Europe. Differences in seasonal precipitation are mostly within ±10 %. In parts of northern Europe, the 2.5 ka climate is up to 30 % wetter in winter than that of PI. In summer there is a tendency for the 2.5 ka climate to be drier than PI in the Mediterranean region.

The results also suggest that LULCC at 2.5 ka significantly impacted the climate in parts of Europe. Simulations including
30   reconstructed LULCC (i.e. those using pollen-derived land cover descriptions) give up to 1 °C higher temperature in parts of northern Europe in winter and up to 1.5 °C warmer in southern Europe in summer than simulations with potential land cover. This relatively strong response implies that anthropogenic land cover changes that had occurred by the late prehistoric period may have already affected the European climate by 2.5 ka.

Climate
of the Past
Discussions

EGU

1 Introduction

35 Increases in the concentration of greenhouse gases in the atmosphere have an impact on the global climate through altering Earth's radiative balance (e.g. Manabe and Wetherhald, 1967). Ruddiman (2003) suggested that humans may have started to affect Earth's climate long before industrialisation and the modern era through human-induced emissions of greenhouse gases, particularly carbon dioxide (CO_2) and methane (CH_4), since the beginning of agriculture (Neolithic cultures). The "Ruddiman anthropogenic hypothesis" challenged the two "natural hypotheses" (i.e. internal processes of the climate system) proposed

40 by Broecker et al. (1999) and Ridgwell et al. (2003), in an attempt to explain the 20 ppm CO_2 increase during the last 7000 years of the current interglacial (the Holocene) that maintained a warm climate, in contrast to the climate history of earlier interglacial periods. The anthropogenic hypothesis has been tested in a large number of studies over the last 20 years, using scenarios of Holocene land-use and land-cover change (LULCC) (e.g. Kaplan et al., 2011), different population growth data (e.g. Boyle et al., 2011) and/or ^{14}C dated archaeological data (e.g. Ruddiman et al., 2016). Few tests have used pollen-based

45 reconstructions of plant cover, although Ruddiman et al. (2016) used a pollen-based reconstruction of vegetation "pseudobiomes" (anthropogenic biomes) *sensu* Fyfe et al. (2015) to provide evidence of sub-continental scale transformation of the vegetation of Europe. Most of the tests have looked primarily on the impact of anthropogenic emissions of CO_2 and CH_4, and none of them have yet been able to reject the anthropogenic hypothesis unequivocally (e.g. see discussions in Stocker et al., 2011 and Ruddiman et al., 2011), and Ruddiman et al. (2016) have added a number of convincing arguments in

50 supporting it.

Both anthropogenic and potential land-cover changes can also influence biogeophysical effects by altering the land surface albedo and roughness (e.g. Field et al., 2007). These effects can have large impacts on regional climate (e.g. Jia et al., 2019), which will affect people directly on a regional to local scale. Such impacts were explicitly shown for Europe in a number of studies with high-resolution regional climate models (RCMs) under present-day conditions (e.g. Belušić et al., 2019;

55 Strandberg and Kjellström, 2019; Davin et al., 2020). For the Mid-Holocene (6000 calibrated years before the present, henceforth abbreviated 6 ka) two studies have investigated the effect of LULCC on the climate of Europe. The first used two different LULCC scenarios (Strandberg et al., 2014) and the second used pollen-based reconstructions of past quantitative land-cover for the first time (Strandberg et al., 2022). Results from these RCM studies indicate that, in southern Europe where an increase in open land cover (herb and low shrub vegetation) at 6 ka can be in large part assigned to human activities, LULCC

60 can have contributed to a change in the average summer temperature of around 0.5 °C. The authors also show that the results are partly model dependent. The response in summer temperature is ultimately decided by the albedo and how the heat fluxes are partitioned between sensible and latent heat. The temperature differences are determined by the model's radiation schemes and land surface physical processes, e.g. the amount of soil moisture available for evapotranspiration.

Although anthropogenic land use by Neolithic cultures impacted the land cover in parts of Europe from ca. 7 ka (e.g. Marquer

65 et al., 2014; 2017), and may have altered the regional climate in various ways (Strandberg et al., 2014; 2021), major episodes of deforestation caused by human impact did not occur before 3000 years later. The most recent pollen-based reconstruction

of land cover in Europe (spatial resolution of 1°; Githumbi et al., 2022) suggests that the earliest of the two major deforestation episodes before the start of Modern time (1500 CE (0.45 ka) – present) took place between ca. 4 ka and 2.5 ka, i.e. the period during which the Bronze Age culture expanded from South-East (Turkey, Greece) to Central and Western Europe

70 (Mediterranean area included) and Northern Europe (Champion et al., 1994; Coles and Harding, 1979). The second deforestation episode (before the Modern time deforestation) occurred ca. 0.9 ka – 0.5 ka, during the Middle Ages (ca. 500 CE (1.45 ka) – 1500 CE in most Europe, started 1050 CE (0.9 ka) in northern Europe)) (Fig. 1a). The difference in open-land cover between 4 ka and 2.5 ka of ca. 10% (either in mean or median cover; Fig. 1a) is assumed to represent deforestation of Europe by Bronze Age cultures. This change in the land cover of Europe was also explained by deforestation for agriculture in the

75 study of Marquer et al. (2017). If we consider a mean natural open-land cover of ca. 20% for the whole of Europe and an increase in open-land cover of a maximum ca. 5% from 7 ka to 4 ka (Fig. 1a), the Bronze Age deforestation corresponds to an increase of open-land cover by 200% since 4 ka. At a broad regional scale, the mean increase between 4 ka and 2.5 ka is also ca. 10 % in each of Europe three major biomes (boreal, temperate and Mediterranean Europe; Fig. 1b-d). At the finer spatial scale (the individual 1° grid cells), the increase ranges from low (or no change) to sometimes much greater conversion of forest

80 to farmland (Githumbi et al., 2022).

Climate
of the Past
Discussions
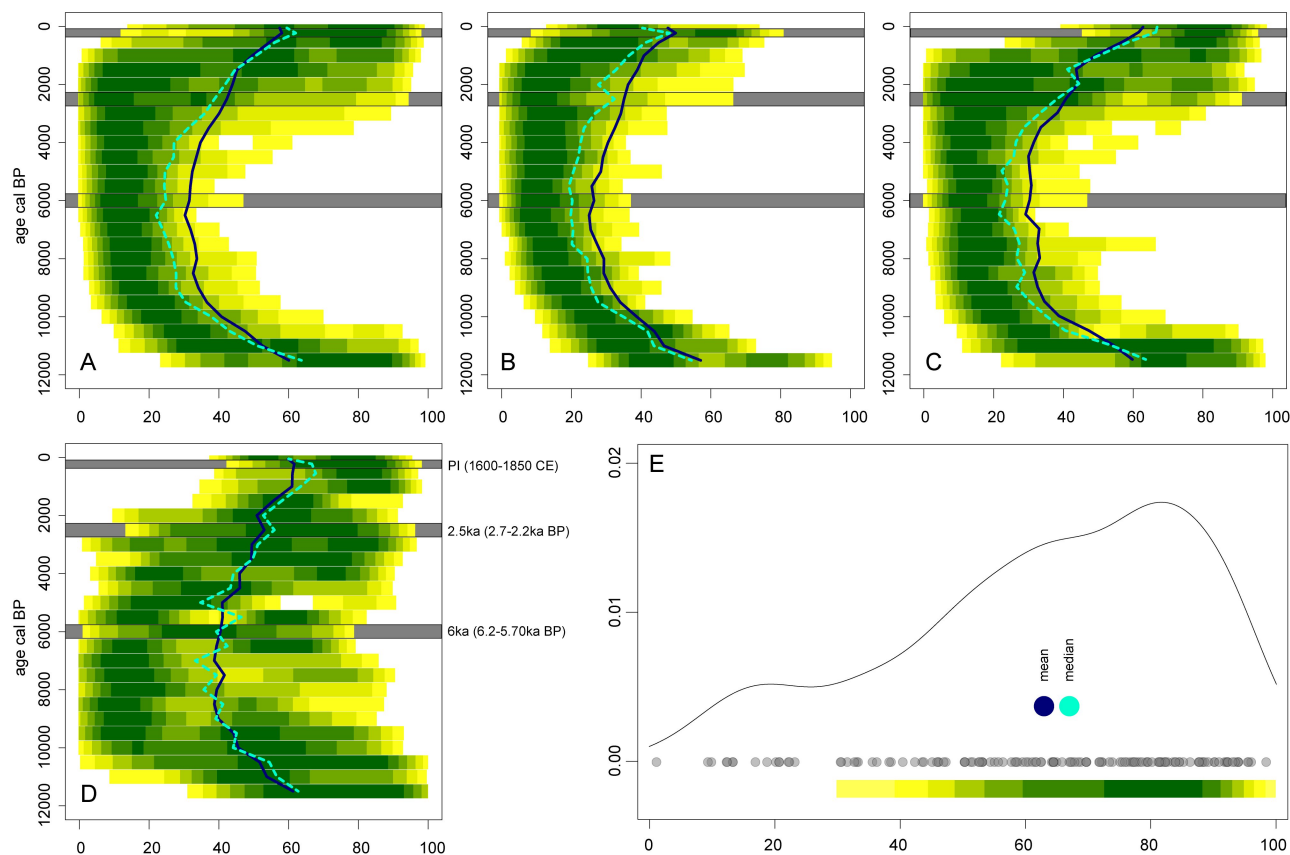
Figure 1: density plots of REVEALS-based open land (% cover) for (A) all European grid cells; (B) the boreal zone; (C) temperate Europe and (D) Mediterranean Europe. Full black lines represent the mean value of open land cover; dashed green lines represent the median value. Panel (E) is illustrative of how the density plots are derived for one time window, showing data values for all grid cells (opaque grey circles), the derived density function as a curve and expressed on the colour gradient, and the mean and median values. Key time intervals (6ka, 2.5ka and PI) are highlighted on panels A-D by the grey bars.

The period around 6 ka is used by palaeoecologists and climate modellers as a representative time slice of the Holocene thermal maximum and the start of agriculture in large parts of the world. It is used broadly in model-data comparison to evaluate climate models against palaeoclimate proxy data (e.g. Braconnot et al. 2012), and to understand and explain the 'Holocene temperature conundrum' (e.g. Bader et al., 2020). However, a better understanding of the possible impact of land use on the Holocene climate since the start of agriculture requires that times of major change in land use are studied. The time around 3 ka (the Bronze Age) was also pinpointed as the time when "the planet [was] largely transformed by hunter-gatherers, farmers, and pastoralists", as suggested by an archaeological global assessment of land use from 10 ka to 1850 CE (ArchaeoGLOBE Project, 2019). Nevertheless, this time period has not been studied specifically by the wider palaeoclimate modelling community so far. In this paper, we are testing the following null hypothesis: the regional climate of Europe around 2.5 ka was significantly influenced by land use via biogeophysical effects due to changes in the properties of the land surface. From a more general perspective, it is also important to understand the biogeophysical effects of LULCC, given that LULCC is affecting most of the Earth's land surface today (Parmesan et al., 2022). Although landscape management is expected to play a large role in the mitigation of climate warming in the future (Nabuurs et al., 2022), the local impact of such mitigation measures on the regional climate and the net effect of both biogeochemical and biogeophysical effects, in the past as well as today, are still not fully understood/known (e.g. Gaillard et al., 2015). The relative importance of LULCC as a climate forcing factor may be large, particularly in low emissions scenarios (van Vuuren et al., 2011).

2 Models and data

2.1 Model chain

This study builds upon a chain of model simulations (see detailed model descriptions below). Within the first step, 2.5 ka and pre-industrial (1850 CE, hereafter PI) climate conditions are simulated by the ocean-atmosphere coupled global model EC-Earth using prescribed PI land cover (Fig. 2 and Table 1). The climate conditions for 2.5 ka are then used to force the DVM LPJ-GUESS over the European domain to simulate the potential land cover consistent with the climate, labelled L (2.5k-L in Table 1). In this context, 'potential' refers to land cover without human intervention. The climate conditions from EC-Earth and the land cover from LPJ-GUESS are used to force the RCMs RCA4 and HCLIM. The RCMs simulate the same periods as the GCM, but at higher horizontal resolution and with their physical parameterisations. For each RCM, the model output includes a high-resolution climate simulation for 2.5 ka and PI respectively (2.5k-L and PI in Table 1).
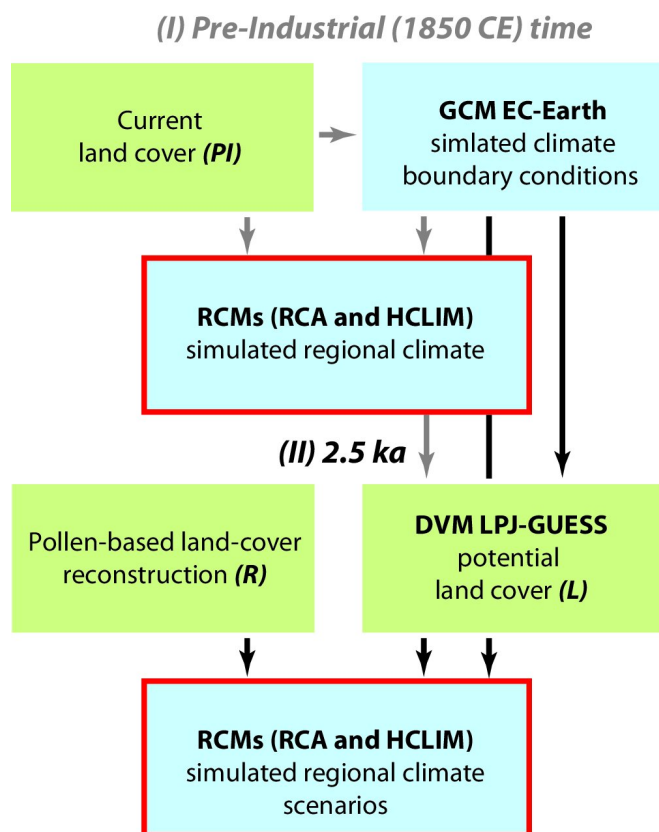
115

(I) Pre-Industrial (1850 CE) time

Current land cover **(PI)**	**GCM EC-Earth** simlated climate boundary conditions

RCMs (RCA and HCLIM) simulated regional climate

(II) 2.5 ka

Pollen-based land-cover reconstruction **(R)**	**DVM LPJ-GUESS** potential land cover **(L)**

RCMs (RCA and HCLIM) simulated regional climate scenarios

Figure 2 Description of the model chain for 2.5 ka. All RCM simulations read boundary conditions from EC-Earth. A first set of simulations are made with current land cover. The EC-Earth climate is used in LPJ-GUESS to provide the 2.5 ka potential land cover (L) subsequently used in the RCMs. A Bayesian spatial statistical model is used to reconstruct 2.5 ka land cover (R) that is also used in the RCMs (see text for details on the pollen-based reconstruction).

120

Land cover (i.e. plant cover) at 2.5 ka was reconstructed at a 1° spatial scale using >1000 pollen records and the REVEALS model (Sugita, 2007; Githumbi et al., 2022). Because pollen records are not available in all grid cells, a spatial statistics method

125 was used to interpolate the pollen-based land cover over the entire grid covering Europe using the approach described in e.g. Pirzamenbein et al. (2018). The method uses additional co-variates, i.e. simulated potential land cover from LPJ-GUESS (driven by the climate from the EC-Earth simulation, Fig. 1) and the KK10 LULCC scenario for 2.5 ka (Kaplan et al., 2009). This spatially continuous land-cover reconstruction is labelled R (2.5k-R in Table 1) and represents the climate- and human-induced land cover.

130 A similar approach was used in Strandberg et al. (2022). Here we use a more straightforward approach where the LPJ-GUESS simulations use the climate from EC-Earth only, instead of also doing an iteration where the RCMs force LPJ-GUESS. Although some studies indicate that more than one iteration between a climate model and the vegetation model are needed to reach equilibrium (e.g. Velasquez et al., 2021), and simulated land cover is sensitive to the representation of climate used and

vice versa (Strandberg et al., 2022), we chose to use only one iteration. This is because the difference between reconstructed

135 and simulated land cover is larger than the differences between alternative simulations of land cover. Contrasting the simulated

potential land cover with the pollen-based reconstruction allows us to explore the effect of LULCC on regional climate. The

only difference between the regional climate simulations is the representation of land cover. This would not be possible to

achieve with coupled DVM-RCM simulations. Therefore, we catch some of the uncertainty by using two different land-cover

representations L and R (Fig. 2). Such sensitivity tests give us the possibility to study the effect of land cover on climate, and

140 how two different RCMs respond to land-cover change. The approach also allows to produce and evaluate a multi-model

estimate of 2.5 ka climate.

Table 1. Combination of models and land cover (LC) used in each simulation. EC-Earth is used as the driving GCM in all simulations. The DVM is driven by climate conditions from EC-Earth and simulates potential LC labelled 'L'. * indicates that
145 the LC is simulated and not a forcing. PI Pre-industrial (1850 CE); R interpolated pollen-based REVEALS land-cover reconstruction (see text for further explanations)

Simulation	Time	RCM	DVM	LC
EC-Earth(PI)	PI			PI veg.
RCA(PI)	PI	RCA4		PI veg.
HCLIM(PI)	PI	HCLIM		PI veg.
EC-Earth	2.5 ka			PI veg.
LPJ-GUESS(L)	2.5 ka		LPJ-GUESS	L*
RCA(2.5k-L)	2.5 ka	RCA4		L
HCLIM(2.5k-L)	2.5 ka	HCLIM		L
RCA(2.5k-R)	2.5 ka	RCA4		R
HCLIM(2.5k-R)	2.5 ka	HCLIM		R

2.2 EC-Earth3.3

The lateral boundary conditions for the RCMs are taken from simulations with the CMIP6 version of the fully coupled general

150 circulation model EC-Earth (Döscher et al., 2022) at T159 horizontal spectral resolution (approximately 1.125° × 1.125°) in

the atmosphere (this particular configuration is named EC-Earth3-LR in CMIP6, where LR stands for low resolution). The

performance of EC-Earth3 when simulating past climate change is evaluated in Zhang et al. (2021). More details on the set-

up used here are given in Strandberg et al. (2022).

We perform the PI and 2.5 ka simulations following the PMIP4 protocol (Otto-Bliesner et al., 2017). The model setup is
described in Zhang et al. (2021). For the 2.5 ka simulation, the climate forcing factors that differ from PI are orbital parameters,
and concentrations of carbon dioxide (CO_2) and methane (CH_4). The orbital forcing for PI and 2.5 ka is calculated following
Berger (1978). The CO_2 concentrations are 284.2 ppm_v (PI) and 276.2 ppm_v (2.5 ka) and those for CH_4 808.2 ppb_v (PI) and
590.6 ppb_v (2.5 ka). All other climate forcing factors (e.g. aerosols) and boundary conditions (i.e. land-sea mask, orography)
are the same in PI and 2.5 ka. The land cover used in the PI and 2.5 ka simulations is prescribed using simulated land cover for
1850 CE from LPJ-GUESS implemented offline. The quasi-equilibrium representing the 2.5 ka climate conditions is reached
after 200 years of simulation.

2.3 RCA4 and HCLIM

Two regional climate models (RCM) are used to downscale the simulations from EC-Earth, thereby adding geographical
details and improving the simulation of climatic processes as the horizontal grid spacing is denser in the applied RCMs (~50
km) than in EC-Earth (~100 km). In this study, the Rossby Centre Atmosphere model (RCA4, Strandberg et al., 2015;
Kjellström et al., 2016) and the HCLIM38-ALADIN (HCLIM, Belušić et al., 2020) are run on a horizontal grid spacing of
0.44° (corresponding to approximately 50 km) across Europe (the CORDEX EUR-44 domain (Jacob et al., 2014)). Both
RCMs have been extensively used for simulations of past and future climates. RCA4 and HCLIM were used in the same set-
up to simulate 6 ka climate (Strandberg et al. 2022). Details on model parameterisations and how the RCMs read data from
EC-Earth can be found in that study.

PI and 2.5 ka are represented by 30-year periods in the RCMs. Differences in temperatures and heat fluxes between the L and
R simulations are tested using a student's t-test with Bonferoni (1936) correction for multiple testing. The resulting procedure
has a 5 % family-wise error rate, i.e. the probability of one or more false positives among all grid cells is 5 % instead of the
5 % false positive rate for each grid cell obtained when no correction is applied. Only significant differences are shown in
Figures 7, 8 and 10).

2.4 LPJ-GUESS

The dynamic vegetation model (DVM) LPJ-GUESS (Lund-Potsdam-Jena General Ecosystem Simulator) used in this study is
an individual-based ecosystem model optimized for regional studies (Smith et al., 2001; Sitch et al., 2003; Smith et al., 2014).
LPJ-GUESS has previously been used with RCA3 (Kjellström et al., 2010; Strandberg et al., 2011; Strandberg et al., 2014)
and RCA4 and HCLIM (Strandberg et al., 2022) for different past climates. LPJ-GUESS shows good performance when
simulating potential land cover in Europe (Lindgren et al., 2021).

LPJ-GUESS simulates the potential land cover for Europe at 2.5 ka using climate forcing (temperature, precipitation, and
radiation) from EC-Earth, and the same CO_2 level as applied in EC-Earth. The land cover input to the RCM is generated by
summing the plant functional types into three land-cover types: summer-green trees (ST), evergreen trees (ET) and open land

(OL) (Table A1). The fraction of the non-vegetated area (or bare land, BL) was estimated by subtracting the summed land cover from one.

2.5 Pollen-based REVEALS estimates of plant cover and their spatial interpolation

REVEALS (Regional Estimates of Vegetation Abundance from Large Sites) is a model that estimates regional plant cover
190 using pollen records (Sugita, 2007). To achieve reconstructions of past land cover that can be used in climate modelling, pollen-based REVEALS estimates of plant cover are produced at a 1° grid scale using all suitable pollen records available in each grid cell (Gaillard et al., 2010; Gaillard et al., 2018). The first REVEALS reconstruction of this kind was performed for Europe (Trondman et al., 2015) and was used to evaluate the LULCC scenarios KK10 and HYDE (Kaplan et al., 2017) and discuss the effect of LULCC on simulated regional climate in Strandberg et al. (2014). For this study and the earlier one on
195 the climate at 6 ka (Strandberg et al., 2022), we increased the coverage of the REVEALS reconstruction southwards to the Mediterranean area and eastwards to western Russia and the Middle East (Githumbi et al., 2022). Because the REVEALS estimates of plant cover are not obtained for all grid cells, it is necessary to perform an interpolation to produce a complete pollen-based land cover at a 1° resolution across Europe. This interpolation applies a spatial statistical model described in Pirzamanbein et al. (2018).

200 The spatial interpolation uses large-scale features consisting of elevation and the LPJ-GUESS land cover fractions adjusted by LULCC at 2.5 ka as derived from the KK10 scenarios (Kaplan and Krumhart, 2011). The correlation between these large-scale features and the REVEALS estimates of plant cover is computed and used for interpolation. It is important to note that by estimating correlations, only the patterns in the features are used for interpolation. The effect on the interpolation of using large-scale features (i.e. LPJ-GUESS land cover) derived from different climate models was small in a sensitivity study
205 (Pirzamanbein et al., 2020), which suggests that a single iteration between the climate model and the vegetation model is sufficient for the spatial interpolation described here. Small-scale spatial patterns in the REVEALS estimates that are not captured by the large-scale features are interpolated by a Gaussian Markov Random Field (Lindgren et al., 2011). The model uses Dirichlet distributions for compositional data (Aitchison, 1986) to ensure that the interpolated land cover fractions are between 0 and 1 and that the total land cover in each grid cell sums to 1.

210 The REVEALS reconstructions and the spatial interpolation provide land cover for vegetated areas, with total land cover summing to 1. To account for bare land (BL), the statistical interpolation is adjusted using the fraction of bare ground in the simulated potential land cover obtained from LPJ-GUESS. The adjustment increases the land-cover type open land (OL) (see LPJ-GUESS modelling above) in sparsely vegetated areas, such as mountainous or dry regions.

To compare the potential and reconstructed landcover used in the simulations we computed differences between each landcover
215 class for each pixel as well as joint measures of distance between the complete landcover compositions for each pixel. Let p_k and q_k be the proportions of land cover in the 4 different classes, indexed by k, for the potential and reconstructed landcover in single pixels. The distances between the two compositions were computed using standard Euclidian distances as,

$$D = \sqrt{\Sigma_k \left(p_k - q_k \right)^2} \qquad \text{(Eq. 1)}$$

220

and using the compositional distance suggested in Aitchison (1992) and Aitchison et al. (2000) as

$$ACD = \sqrt{\Sigma_k \left(log\left(\frac{p_k}{\sqrt[K]{\Pi_l\, p_l}} \right) - log\left(\frac{q_k}{\sqrt[K]{\Pi_l\, q_l}} \right) \right)^2} \qquad \text{(Eq. 2)}$$

225   where K in the root is the total number of classes (K=4 here).

Compared to the Euclidian distance the Aitchison compositional distance (ACD) puts greater emphasis on relative differences between compositions. As an example, if the landcover fractions change from 40% evergreen, 20% summergreen, 20% open land, 20% bare land to 49%, 17%, 17%, 17% respectively the relative abundance of the last three classes stays the same (they are each 1/3 of the remaining landcover) and the ACD will correctly account for this. As a consequence of this focus on relative

230   differences an increase from 1% to 2% will be seen as very similar (but not identical) to an increase from 10% to 20% (both represent a doubling of that composition). Thus the ACD shows larger differences for areas where one, or more, compositions are very rare.

235   **3 Results**

3.1 Potential and reconstructed land cover at 2.5 ka

Below, potential land cover (L) is the climate-induced land cover at 2.5 ka simulated by LPJ-GUESS using the EC-Earth derived climate. Reconstructed land (R) is the interpolated pollen-based REVEALS-estimated plant cover, i.e. both climate- and human-induced land cover (Fig. 2 and Table 1).

240   Potential land cover (L) is dominated by evergreen trees (ET) in northern and eastern Europe (Fig. 3). Summer green trees (ST) prevail in western Europe, and mixed evergreen and summer green woodland (ET + ST, orange colours) occupy the hemiboreal zone (between the boreal and temperate biomes) starting in southern Norway and becoming larger eastwards over southern Sweden, the Baltic countries and Russia, and an area in the lowlands north of the Alps that meets the hemiboreal zone in Poland. Most mountainous areas of south-central Europe (Alps, Carpathians, Caucasus) have higher ET proportions than

245   the surrounding plains. At high elevations and latitudes, the Scandinavian mountains are characterised by a higher proportion of open land cover (OL) and bare land (BL) than at lower elevations and latitudes, at the expense of trees. Besides those areas,

OL proportions are negligible in most of northern and central Europe. OL, often with high BL proportion, has its largest proportions on the western fringe of Europe and in the south-eastern part of the continent.

The reconstructed land cover (R) shows similar spatial patterns of tree cover to those in the potential land cover, with ET

250   dominant in northern Europe and the mountainous areas of northern and central Europe, and ST largest proportions at low latitudes in central and western Europe. However, the proportions of mixed ET and ST woodland and ET/ST mixed with OL in the reconstructed land cover (R) are much larger than in the potential land cover (L).

Both standard Euclidian distances (ED) and Aitchison compositional distances (ACD) (Fig. 3) show that the largest differences between R and L land cover are found in the westernmost parts of Europe in westernmost Norway, Ireland, Britain, western

255   France, and northern Spain. ACDs are larger than EDs for areas where one, or several, land-cover types have small % cover (section 2.5), which is the case in Ireland and northernmost Britain. In contrast, EDs are larger than ACDs where none of the land-cover types have very low % cover (most of northern, central, and eastern Europe). Difference maps (R-L) for the three land-cover types (ET, ST, and OL), BL being the same in both R and L (Fig. A1), provide information on which land-cover type(s) most influence the differences between R and L. ET cover is smaller in R than in L land cover (- 10% to - 40%) in most

260   of Boreal and northernmost Europe, in particular along the Norwegian coast (up to – 40% to - 80%), while it is larger in R than in L (+10% to +40%) in the southern part of temperate and Mediterranean Europe, and more so in western Spain, SW France, the French riviera, Italy, and an area in eastern Europe from the Czech Republic down to Greece and western Turkey (+ 20% to + 40%). ST cover is smaller in R than in L land cover in temperate and Mediterranean Europe, especially in Spain, France, and the British Isles (- 60% to - 80%), while it is larger in R than in L mainly along the coasts of Boreal and northernmost

265   Europe (+ 10% to + 20%). OL cover is larger in R than in L in most of Europe (mainly + 10% to + 40%; ≥ 40% in W Europe) except in an area from Hungry down to northern Greece, Bulgaria, Romania, and Central Turkey where R-L is around zero or -10% to - 40%. The largest R-L differences in OL are found in NW Spain, NW France, the British Islands, and the north-western coast of Norway (+ 40% to + 60 (80)%) and in NE Greece, central Romania, southern Russia (Volgograd area), and western Kazakhstan (- 20% to – 40%).
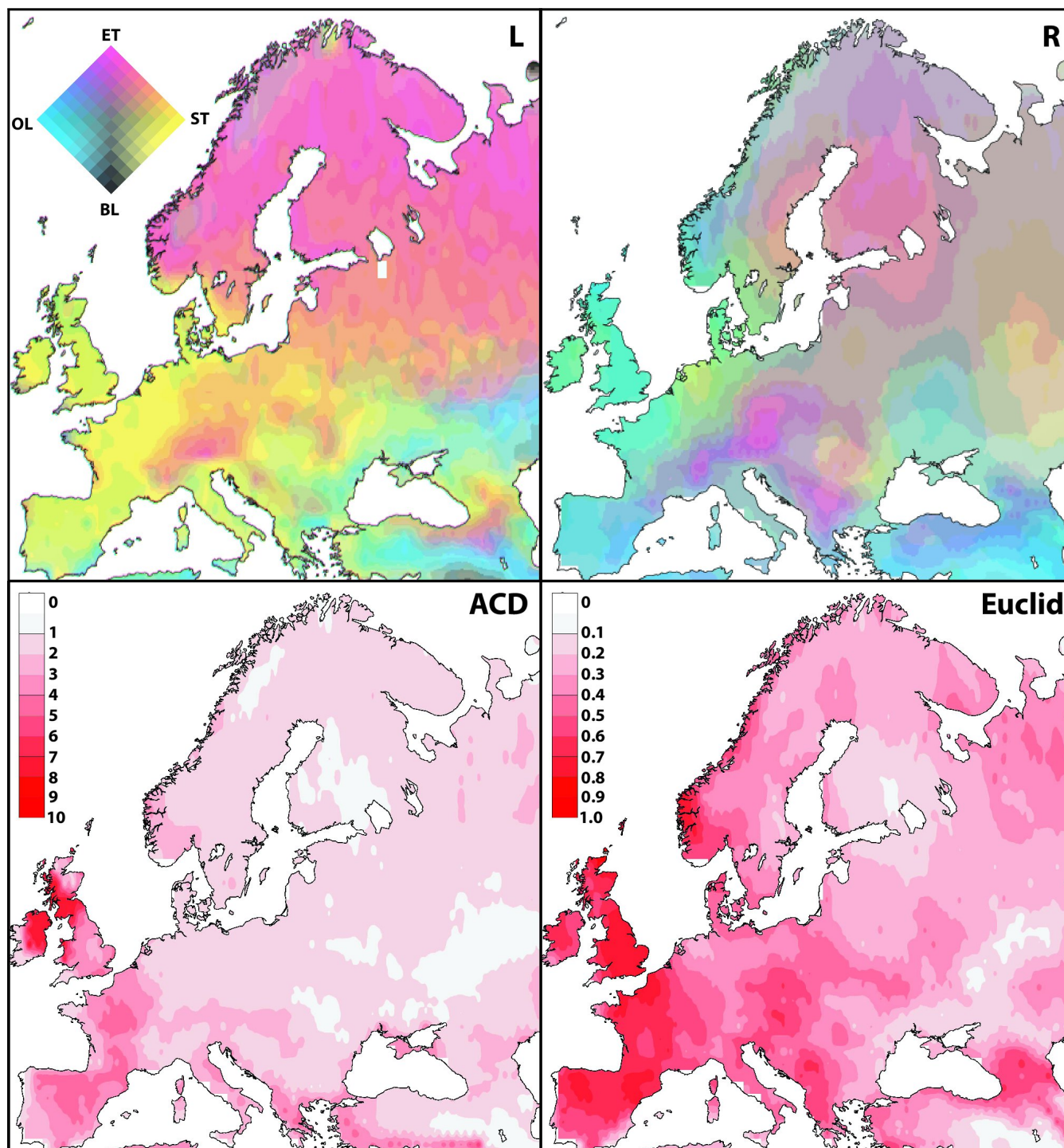
270

Climate
of the Past
Discussions

Figure 3 Upper panels: Composite maps of (L) LPJ-GUESS simulated potential land cover using climate input from EC-Earth and (R) interpolated pollen-based REVEALS estimated land cover in Europe at 2.5 ka. Legend: ET - evergreen trees; ST – summergreen trees; OL - open land; BL – bare land. Lower panels: Two measures of the difference between the composite maps L and R,

Climate
of the Past
Discussions

275 **Aitchison's compositional distance (left) and Euclidian distance (right). The darker the red, the greater the difference in land-cover composition between the maps. See text under methods and results for details.**

3.2 Simulated climate

Figures 4 and 5 show the differences between the simulated 2.5 ka and PI temperature (at 2 m above surface) and precipitation, respectively, in winter and summer. Here we first describe the results for the 2.5k-R runs because they use land-cover data
280 inferred from empirical proxies of past land cover, i.e. pollen-based REVEALS estimates of plant cover, so far the best possible reconstruction of actual land cover in the past (e.g. Trondman et al., 2015; Kaplan et al., 2017; Roberts et al., 2018; Githumbi et al., 2022). We describe the impact of different land-cover data on climate in section 3.3. Henceforth, the difference of temperatures or precipitations between 2.5 ka (with land cover R in both RCMs) and PI are abbreviated (T 2.5k – PI) and (P 2.5k – PI) respectively. Note however that the EC-Earth simulations do not use the land-cover data R for 2.5 ka, but prescribed
285 land cover for 1850 CE. As expected, the general similarities between the GCM and the RCMs simulated climates are larger over the ocean, where the model resolution is less important, and smaller over land, where the land surface is treated differently in the GCM and the RCMs.

In winter, all simulations indicate that 2.5 ka was warmer than PI and show a similar pattern, with the smallest temperature differences between 2.5 ka and PI (T 2.5k – PI) on the Iberian Peninsula (0-1 °C) and the largest ones in north-eastern Europe
290 (4- >6 °C) (Fig. 4). The RCMs exhibit similar patterns as EC-Earth, however with smaller (T 2.5k – PI) with ca. 0.5 °C on the Iberian Peninsula. Moreover, HCLIM shows smaller (T 2.5k – PI) than EC-Earth and RCA4 in most of central Europe. In summer, the smallest (T 2.5k – PI) are also found on the Iberian Peninsula and in western Europe, while the largest (T 2.5k – PI) occur in the northern parts of the domain, especially in areas close to the sea-ice margin in the far north (Fig. 4). The difference in (T 2.5k – PI) between RCA4 and HCLIM is larger in summer, although patterns are similar. While (T 2.5k – PI)
295 are 1-2 °C in the HCLIM simulations, they are close to zero in central and eastern Europe in the RCA4 ones. Both RCMs simulate a (T 2.5k – PI) of 0.5 to 1.5 °C in the eastern and northern parts of the domain, which is less than in EC-Earth.
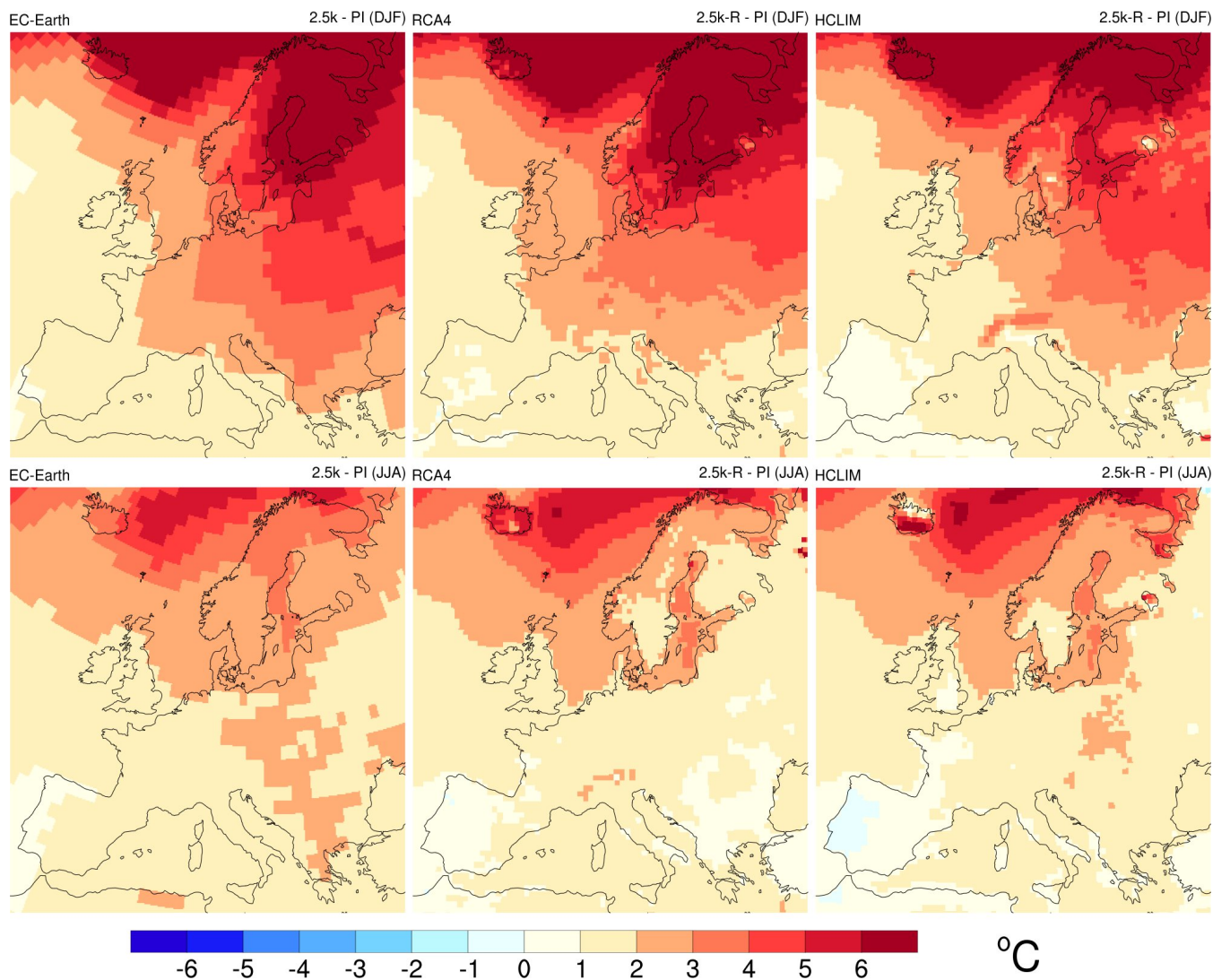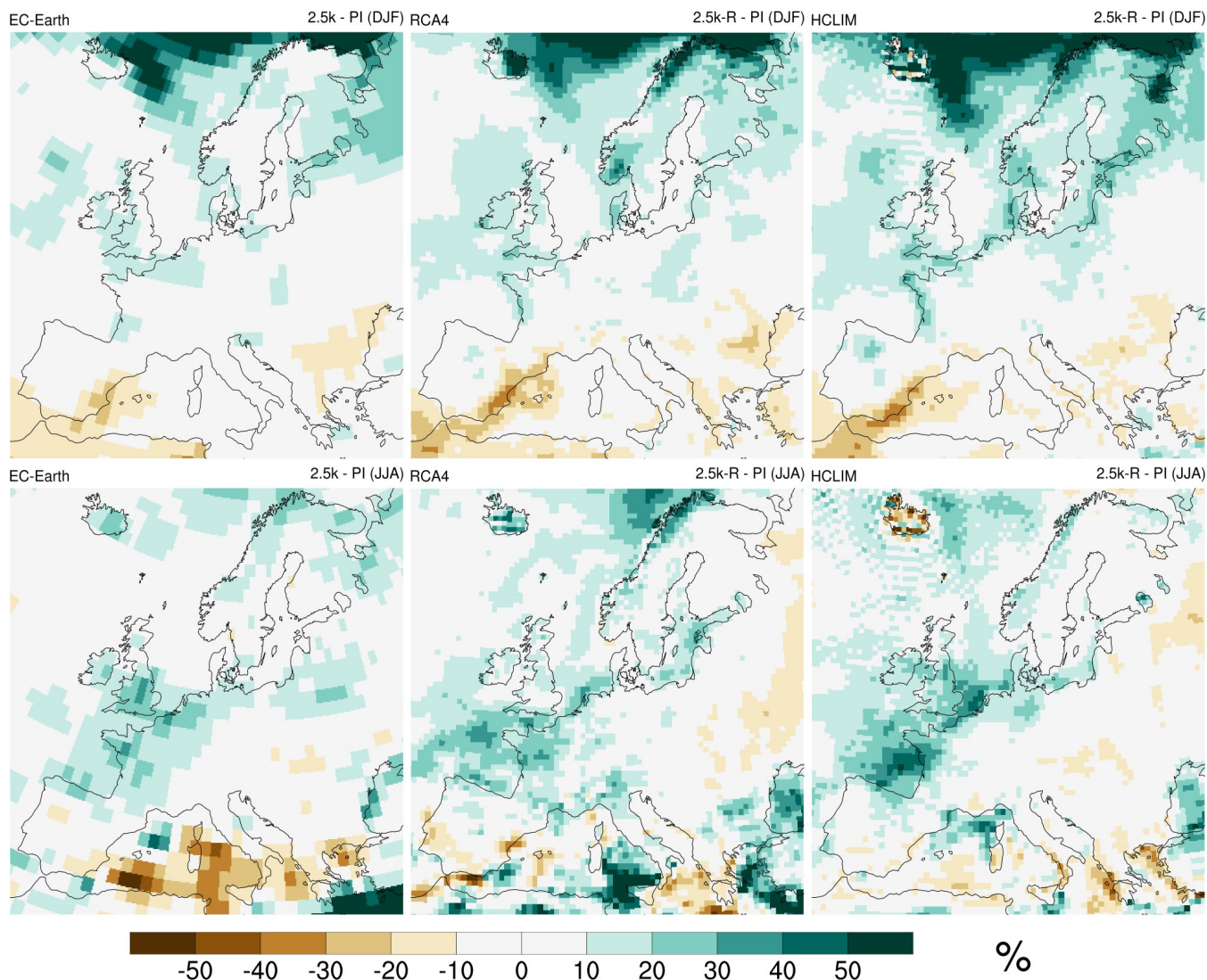
Figure 4 Temperature difference (°C) between 2.5 ka and PI (T 2.5k-R – PI) for winter (DJF, top row) and summer (JJA, bottom row) as simulated by EC-Earth (left), RCA4 (middle) and HCLIM (right).

300

Overall, and in both winter and summer, the difference in precipitation between the two time periods (P 2.5k – PI) is small (within ±10 %), except for areas close to the northern rim of the domain in winter, where 2.5k-R is wetter than PI with (P 2.5k – PI) ≥50 % in all models (Fig. 5). Most regions in central Europe and the Mediterranean are characterised by low positive or negative (P 2.5k – PI) (up to ±10 %). All three models show similar precipitation patterns, which suggests that precipitation is

305 mainly governed by the large-scale circulation as simulated by the driving GCM. However, there are notable differences in (P 2.5k – PI) between the RCMs and EC-Earth, which suggests that changes in the precipitation amount results also from local processes including small-scale convection.

13

Figure 5 Precipitation difference (%) between 2.5 ka and PI (P 2.5k-R – PI) for winter (DJF, top row) and summer (JJA, bottom row) for EC-Earth (left), RCA4 (middle) and HCLIM (right).

Figure 6 shows sea level pressure (SLP) at PI and the difference between 2.5 ka and PI (SLP 2.5k – PI). In winter, the RCMs show similar patterns as EC-Earth, however with in general slightly lower pressure over the continent. Comparing the two time periods, it is clear that SLP is lower at 2.5 ka over Scandinavia, the British Isles and the North Atlantic, which implies enhanced cyclone activity. Lower SLP values at 2.5 ka than PI occur farther south, and are more common over Scandinavia, in EC-Earth than in the RCM simulations. Such differences between the RCMs and the driving GCM partly explain differences in (P 2.5k – PI) between the models and between time periods. For instance, the negative SLP difference in Scandinavia and the North Atlantic may be related to that region's larger positive precipitation difference (Fig. 5).

14

In summer, the simulated mean sea level pressure patterns in PI are similar between EC-Earth and the RCMs. It is also clear

320   that differences between the two periods (SLP 2.5k – PI) are generally small, which may contribute to the small differences in

precipitation (P 2.5k – PI) between the periods (Fig. 5). The RCMs show higher SLP in 2.5k over Scandinavia, as opposed to

EC-Earth. Potentially, the lower SLP in EC-Earth may be representative for the positive (P 2.5k – PI) in the area east of the

Baltic Sea where the RCMs show small, or even negative (P 2.5k – PI).
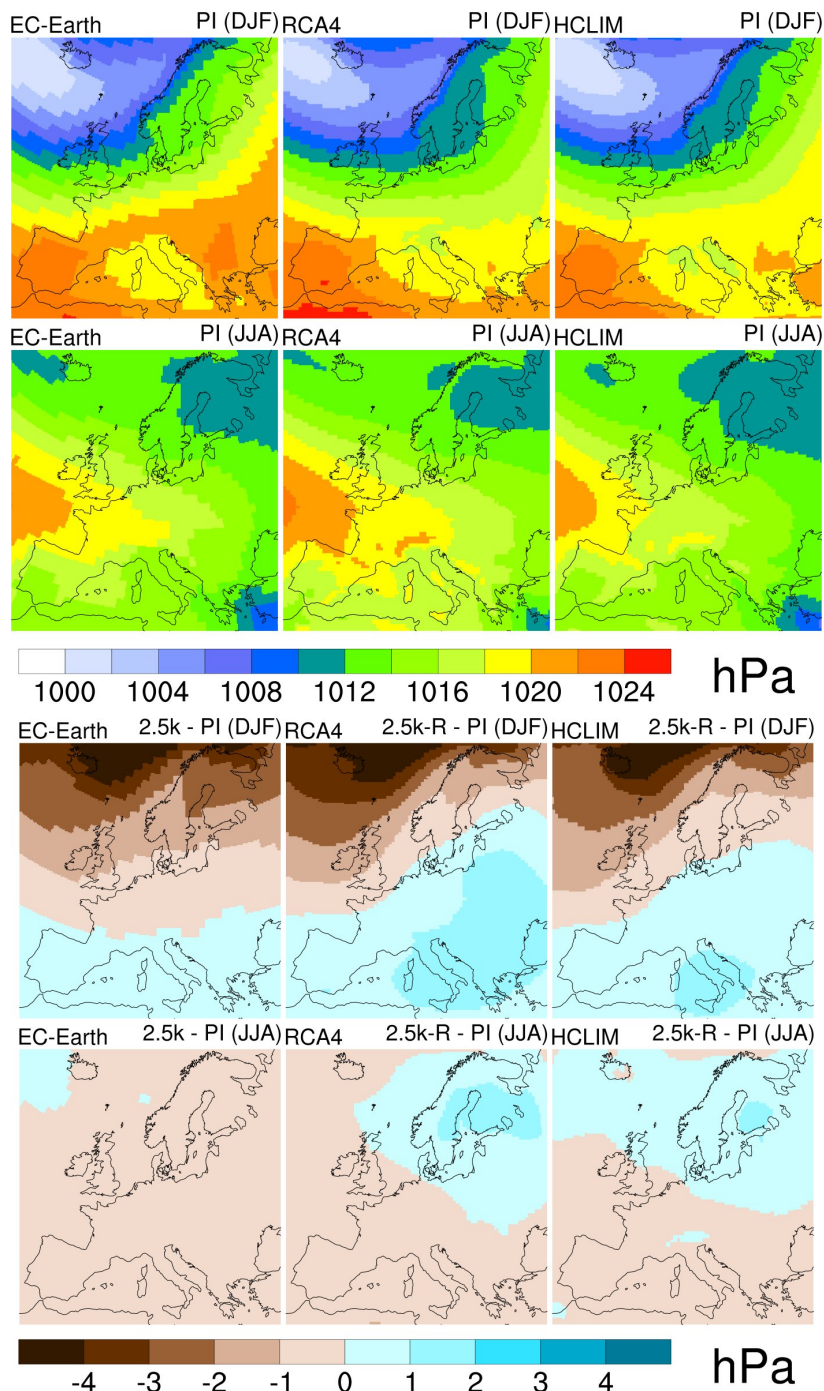
Figure 6 PI sea level pressure (hPa) in winter (DJF, first row) and summer (JJA, second row). Difference in sea level pressure (hPa) between 2,5k-R and PI in winter (DJF, third row) and summer (JJA, fourth row). EC-Earth (left), RCA4 (middle) and HCLIM (right).

3.3 Climate response to differences in land cover- the effect of human-induced land cover

330   In this section, the RCM 2.5k-R runs described in section 3.2 are used as the reference and compared with the 2.5k-L runs, i.e. Figure 7 shows the difference in climate at 2.5 ka resulting from changing land-cover from the potential (climate-induced) land cover (L) to the pollen-based reconstructed land cover (both climate- and human-induced) (R) (see Method section and Figure 2). The difference is expressed as (2.5k-R) − (2.5k-L), henceforth abbreviated R-L (Table 1). Here we present the surface temperature instead of the diagnostic 2 m-temperature, the latter being defined in different ways depending on the

335   model (Breil et al., 2020), while surface temperature has a standard definition (Fig 7).
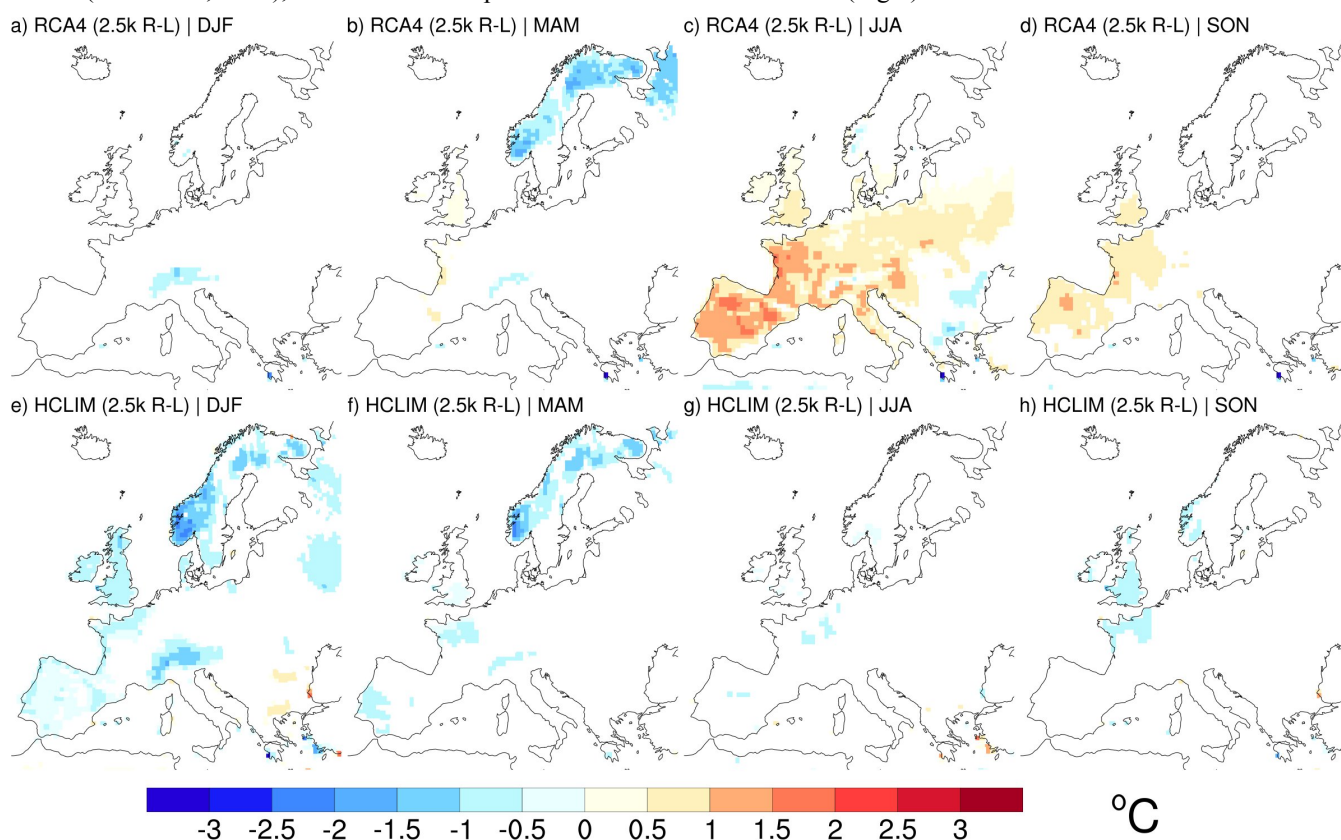
Figure 7 Difference (2.5k R-L) in surface temperature (°C) in RCA4 (a – d) and HCLIM (e – h) for winter (DJF; a, e), spring (MAM; b, f), summer (JJA; c, g) and autumn (SON; d, h). Only grid cells that show a significant difference on a 0.05 level are coloured.

340   In most of the area temperature differences are not significant except for some areas, most notably for HCLIM. In winter the R-L temperature differences are negative (-1 to -0.5 °C) over the Alps in both RCMs (Fig. 7a, e). HCLIM simulates larger R-L temperature differences than RCA4 in large parts of Scandinavia and western Europe, suggesting a stronger sensitivity of HCLIM than RCA4 to the difference in land-cover data. Also in spring, differences are small. A common feature for both

17

RCMs is that R-L temperature differences are negative (-3 to -1 °C) in large areas in Scandinavia including the mountain range
345 (Fig. 7b, f).

In summer, RCA4 responds strongly to the inferred land-cover differences. The R-L temperature difference is 0.5-2°C in southwestern Europe (Fig. 7c, g). HCLIM, on the other hand, shows very small R-L temperature differences. The only significant differences are seen over limited regions in western Europe, and over scattered points in the Iberian Peninsula and along coastal areas in the southeast.

4 Discussion

4.1 Differences in land-cover descriptions

Simulated potential (L) and pollen-based reconstructed (R) land cover exhibit compositional differences (Figure 3, description in Results). Major differences between LPJGUESS-simulated Holocene vegetation and pollen-based REVEALS reconstructions of land cover were discussed in a study using 19 pollen records along N-S and W-E transects through Europe
355 (Marquer et al., 2017) based on pollen-based REVEALS reconstructions of open-land cover. Other earlier studies have compared the results of DVM simulations in Europe with pollen-accumulation rates and pollen percentages (e.g., Miller et al., 2008), or pollen-based REVEALS estimates of land cover (e.g., Pirzamanbein et al., 2014).

It must be kept in mind that the prescribed simulated climate entirely determines the DVM simulated potential land cover in this study, i.e., the simulations do not account for the effects of LULCC. The reconstructed land cover is a pollen-based
360 reconstruction of the climate- and human-induced land cover, i. e. a product of complex interactions between several natural and anthropogenic factors. Disentangling climate- from human-induced pollen-based vegetation is a challenge. Marquer et al. (2017) used a novel approach including the use of variation partitioning to quantify the percentage of variation in vegetation composition explained by climate and land-use variables. The results suggest that climate is the major driver of vegetation when the Holocene is considered as a whole or at a sub-continental scale, but land use appears to be important regionally. Land
365 use becomes a major control of vegetation from ca. 4.5 ka although climate is still the principal driver; however, its influence decreases gradually. Land use is the cause of the more or less continuous increase in OL and decrease in ST from ca. 7 ka (southern Europe) and 6 ka (temperate and most of boreal Europe) until 1850 CE (e.g., Marquer et al., 2014, 2017; Githumbi et al. 2022). However, changes in pollen-based OL do not necessarily represent LULCC but may be due to climate-induced land-cover changes such as spread or decrease of open wetland areas as a consequence of water-level changes (e.g. Pinke et
370 al., 2017). Pollen from the plant families Poaceae (grasses) and Cyperaceae (sedge family) are either difficult or impossible to identify to genera or species, which hampers categorization into dry-fresh and wet meadows, i.e., all types of open land, natural or human-induced, include large amounts of Poaceae and/or Cyperaceae. Consequently, pollen-based OL cover may overestimate human-induced land-cover change. In contrast, cropland (or agricultural land, AL in e.g., Trondman et al., 2015), also included in OL, is always underestimated in pollen-based AL cover as it is represented by cereals only. This is because
375 pollen productivity estimates are not available so far for other crops, and/or the pollen grains of many crops are not

distinguishable from the pollen of wild species belonging to the same plant genera or families. Further details on the interpretation of OL cover in terms of human-induced vegetation openness can be found in Trondman et al. (2015). Despite these issues, it is assumed that most of the increase in pollen-based OL cover since the start of the Neolithic period is human-induced, and that OL cover before the introduction of agriculture was in general < 20% (ca. 10-20%; Fig. 1).

380 Differences between R and L land cover could, besides LULCC, be caused at least partly by differences between the "actual" climate (responsible for the climate-induced part of pollen-based vegetation) and the model-simulated climate. Causes of differences between R and L other than discrepancies in climate and LULCC include processes involved in tree migration (e.g. the Holocene migration lag in *Picea* and *Fagus*: Giesecke and Bennett, 2004; Giesecke et al., 2007; Giesecke et al. 2017) and soil development (e.g. Miller et al., 2008). In spite of continuous progress in effectively modelling such processes in

385 DVMs/ecosystem models, it is not yet implemented as a routine (Lehsten D. et al., 2014, Lehsten, V. et al. 2019). Lower ET values in R than in L land cover in most of northern Europe at 2.5 k BP are partly due to too large abundances of *Picea* in the LPJGUESS simulation.

4.2 Response in the RCMs to land-cover changes

The temperature response to different land-cover data in winter and spring results from the snow albedo feedback and the

390 insulating impact of the snow cover. Open land generally has a higher albedo than forests. Open land is also more readily covered by snow which makes the differences in albedo between open land and forest larger during the snow season. Thus, the temperature response is expected to be the strongest in regions of high altitude or high latitude where there is snow in winter and where the fraction of open land is relatively large.

At high latitudes the amount of incoming solar radiation is small in winter making the snow albedo response weak. The only

395 model consistent R-L temperatures in winter are seen over the Alps. In the Scandinavian mountains, the snow season is long, stretching through spring. Here, the temperature response is stronger in spring when the amount of incoming radiation is larger, even though the difference in albedo between 2.5k-R and 2.5k-L is smaller in spring than in winter (Fig. 7a, b, e, f; see also Fig. 9). The response in temperature to land-cover differences is coherent with the differences in albedo in winter (Fig. 8a ,b). The differences in albedo follow closely the differences in land cover, since land cover to a large extent determines albedo.

400 This agrees with earlier studies of idealised land-cover changes in RCMs showing that albedo explains a large part of the temperature signal in winter in Scandinavia (Strandberg & Kjellström, 2019; Davin et al., 2020).
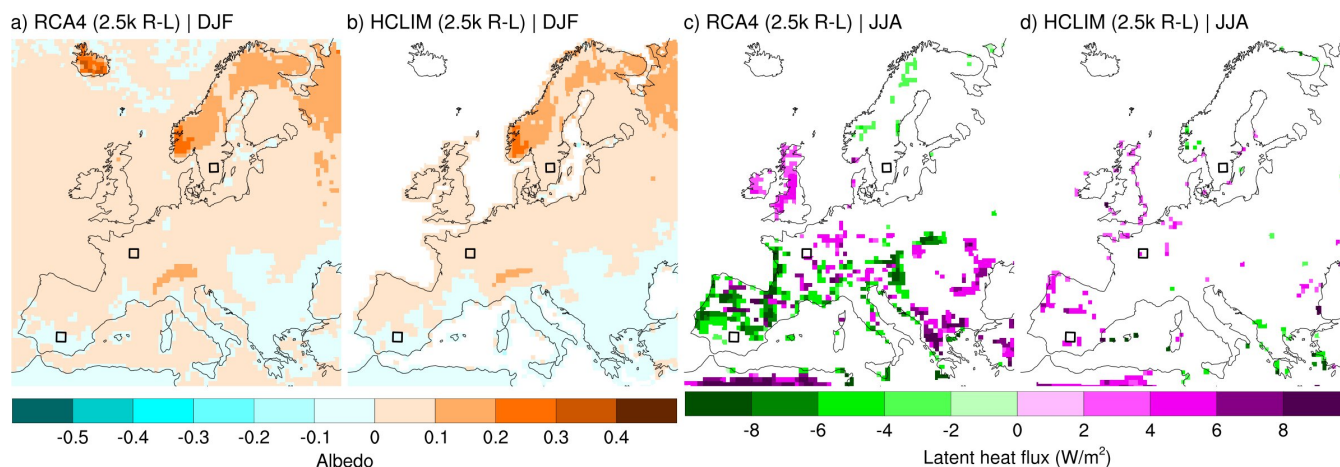
Climate
of the Past
Discussions

Figure 8 Difference between 2.5k-R and 2.5k-L in albedo in winter (DJF) for a) RCA4 and b) HCLIM and in latent heat flux in summer (JJA) for c) RCA4 and d) HCLIM. Black squares show the areas representing Scandinavia (SCA), West Central Europe (WCE) and the Iberian Peninsula (IBP). For latent heat flux only grid cells that show a significant difference on a 0.05 level are coloured.

The areas with the largest R-L temperature differences in summer (Fig. 7c, d, g, h) correspond to the areas with the largest significant differences in latent heat flux as simulated by RCA4 (Fig. 8c). Trees have deeper roots and more leaves than grass, which implies more evapotranspiration (EVT). A more open landscape, such as 2.5k-R, is expected to be warmer in summer due to decreased EVT. In contrast, HCLIM shows few significant temperature differences, as a result of very small differences in latent heat flux (Fig. 8d). Davin et al. (2020) demonstrated that RCMs could disagree in their temperature response to idealised changes in land cover in summer. There is not a direct relationship between differences in land cover and simulated changes in EVT. EVT is determined in the models by the magnitude of land-cover differences, as well as the absolute amount and type of vegetation. Furthermore, local conditions, such as available soil moisture, determine how much water is available for EVT. How these factors are translated into temperature responses depends on the individual models' physics and parameterisations.

To better understand the relationships between surface albedo, latent heat flux and temperature, we present the annual cycles in absolute values for three different small regions (3×3 grid points) representing Scandinavia (SCA), west central Europe (WCE) and the Iberian Peninsula (IBP) (regions shown in Fig. 8). Overall, all four simulations (RCA4 and HCLIM with R or L land cover) agree in terms of shape and amplitude of the annual cycles (Fig. 9). The largest discrepancies between RCA4 and HCLIM are in the annual cycles of EVT in WCE and IBP. In WCE RCA4 simulates a larger amplitude and slightly higher values of EVT in the second half of the year. In IBP, it is HCLIM that simulates a larger amplitude and a longer period of high EVT. Trees have a longer period of EVT than herbs, but not necessarily a higher annual maximum of EVT (Kelliher et al., 1993; Strandberg & Kjellström, 2019). Resulting differences are seen for WCE and IBP in RCA4, and to some extent HCLIM simulations. A possible explanation for the higher latent heat fluxes in the 2.5k-R runs is that grasslands do not retain water as efficiently as woodlands, which would mean that the latent heat flux increases faster and reaches higher levels, to then drop

faster. Such a pattern is seen in both RCA4 and HCLIM simulations, but it is clear that RCA4 tends to dry out more rapidly than HCLIM (Fig 9f).
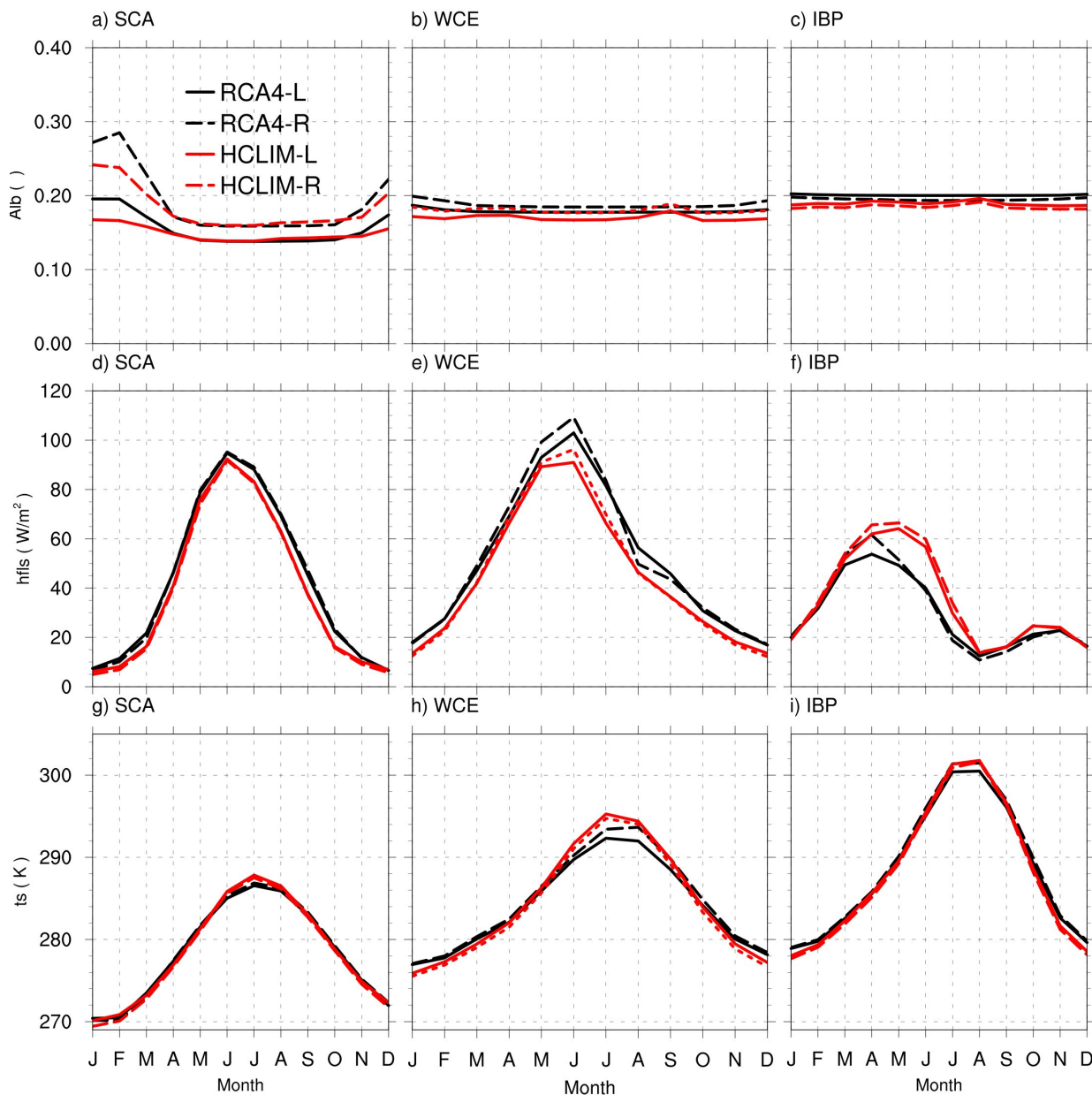
430

Figure 9 Annual cycles of surface albedo (alb; a-c), latent heat flux (hfls (W m⁻²); d-f) and surface temperature (ts (K); g-i) for Scandinavia (SCA; a, d, g), West Central Europe (WCE; b, e, h) and the Iberian Peninsula (IBP; c, f, i). Data from RCA4 are represented by black lines, data from HCLIM by red lines. Simulations using potential land cover from LPJ-GUESS are labelled

435 **with 'L' and shown as full lines, and those using pollen-based REVEALS reconstructed land cover are labelled with 'R' and shown as dashed lines.**

4.2 RCM simulated climate compared to proxies

To evaluate the climate-model simulations, we compare simulated temperatures to proxy data from the Temperature 12k Database (Kaufman et al., 2020). We let all proxy data represent the overall patterns of 2.5 ka temperature and compare that with the overall patterns from the models. Figure 10 shows winter and summer temperatures at 2.5 ka as given by proxy data

440 and the climate models with R land cover in this study.

In winter, there is a general agreement among the models that temperatures range, along a northeast to southwest gradient, from -10 °C and below in northeastern Europe to around 5 °C in the Iberian Peninsula. There is also agreement that eastern Europe is colder than western Europe at the same latitudes, and that the Scandes mountains, the Alps and the Carpathians are colder than the surrounding areas. Compared to proxies, the models are colder on Iceland, except perhaps HCLIM, and warmer

445 along the coasts of western Europe and parts of central and eastern Europe. In summer, there is a general agreement that temperatures range from around 10 °C in the north to approximately 24 °C in the south. Compared to proxies, the models are warmer in Iceland and central eastern Europe, especially in EC-Earth.

Even though there is general agreement between models and proxies there are also differences. Some proxies show considerable differences to the model data, and even if proxies and data have the same colour in Fig. 12, the difference may

450 be up to 2 °C. In addition, the proxy data is not internally consistent, which makes it difficult to know how good they are for comparison with models. The proxy data come from lake sediment, marine sediment, peat, glacier ice, and other natural archives, made with different methods and varying uncertainties (Kaufman et al., 2020). Making an in-depth model-proxy comparison would require an assessment of each data point (what they represent, uncertainty ranges etc.) and it is outside the scope of the paper. For this study, it is sufficient to conclude that the models give a picture of 2.5 ka temperatures that largely
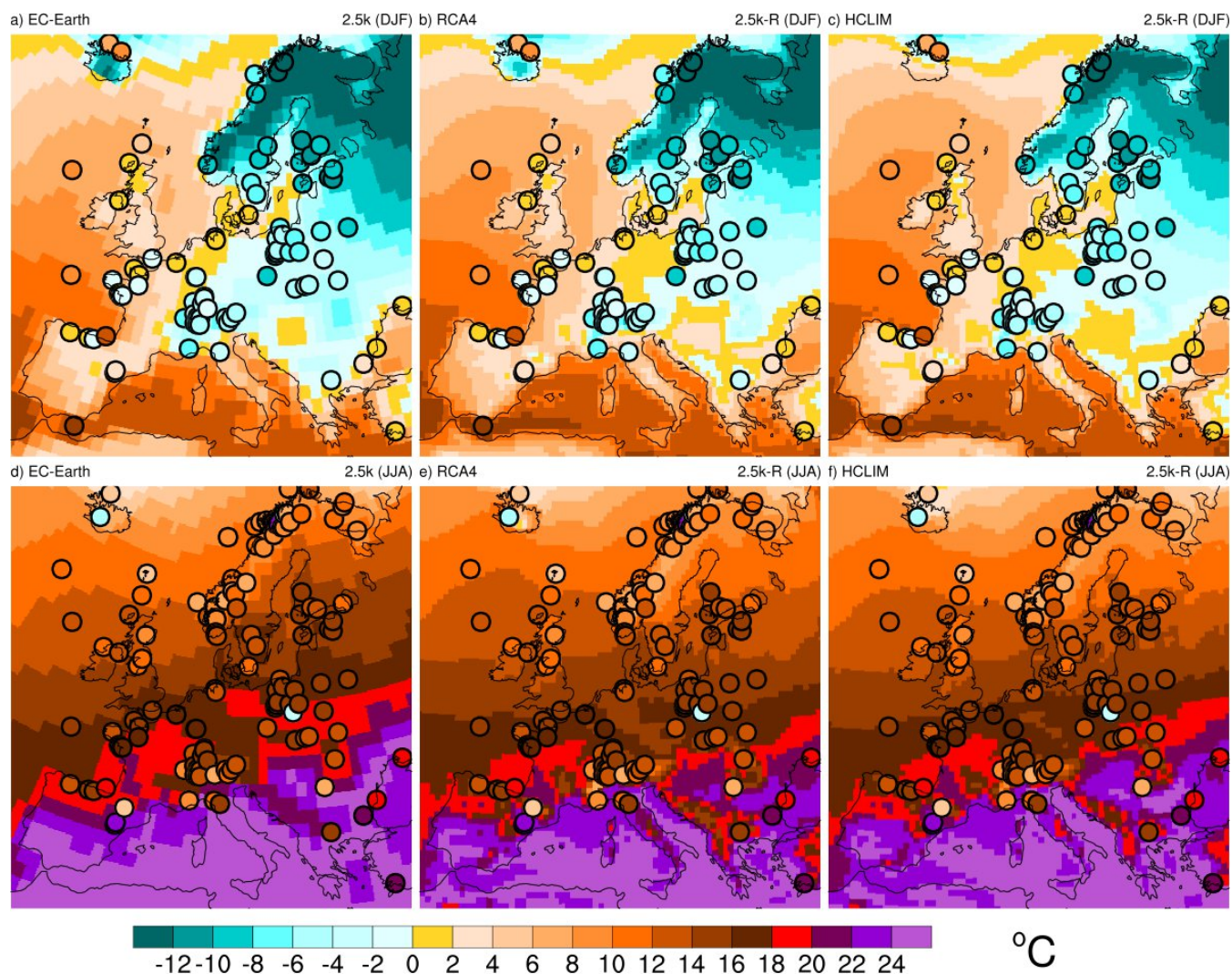
455 agrees with that from proxy data.

Fig 10 Temperature (°C) at 2.5 ka in winter (DJF, top row) and summer (JJA, bottom row) as simulated by EC-Earth (left), RCA4 (middle) and HCLIM (right). Proxy data are shown as circles.

To decide whether the inclusion of reconstructed land cover improves the comparison with proxy data, we compare each proxy

460   data point with the value from the corresponding grid cell in all four RCM simulations. Figure 11 shows how the proxy data

correlate to the simulated temperature in HCLIM in winter and summer. The general agreement between models and proxies

seen in Figure 10 is seen also here as fairly strong correlations both in winter and summer. The differences between HCLIM-

L and HCLIM-R are small, both the root mean square error (RMSE) and the correlation coefficient are more or less the same

for both simulations (Table 3). RCA4 and EC-Earth also give similar values.
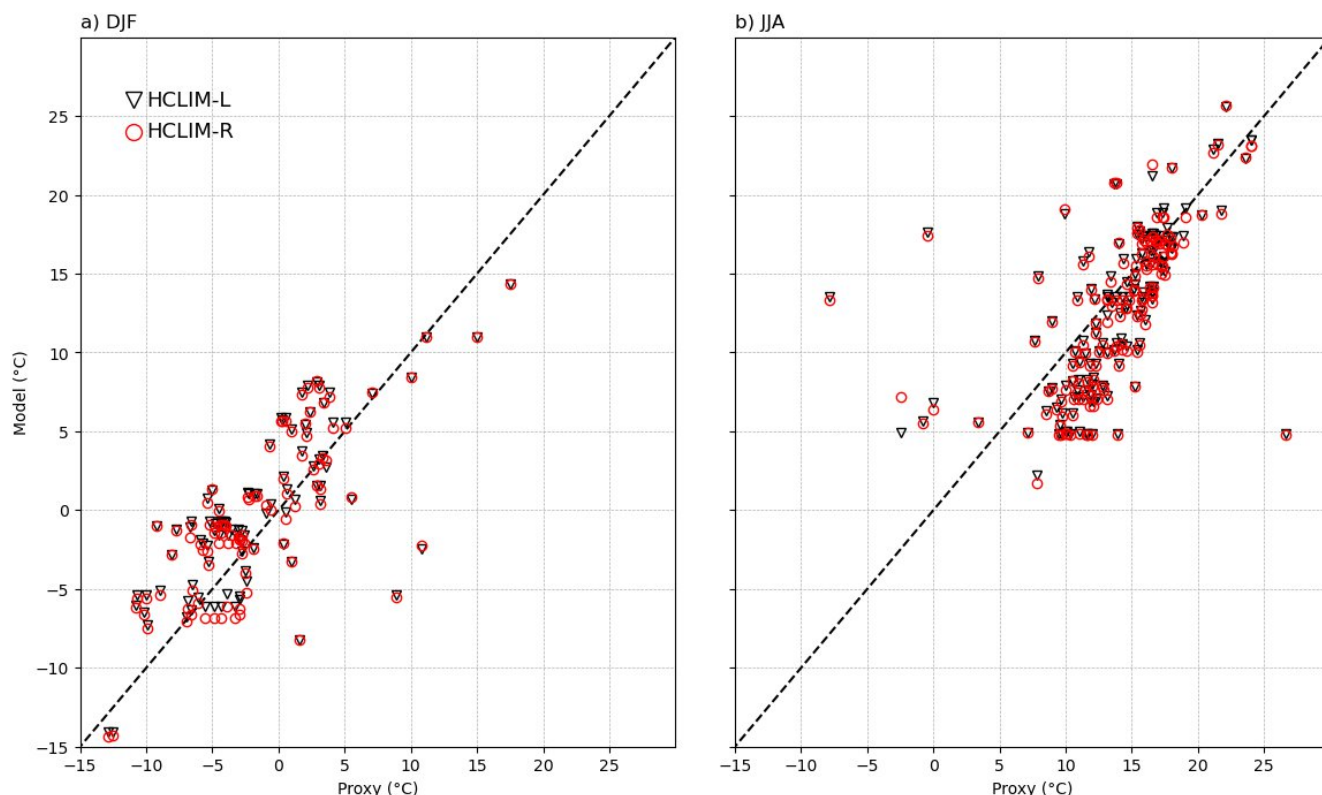
465

Figure 11 Simulated (y axes) and proxy (x axes) temperatures at 2.5 ka in winter (a) and summer (b). Temperatures from HCLIM-L are represented by black triangles, and from HCLIM-R by red circles. The locations of the data points are seen in Fig 12.

It is a challenge to assess the effect of adding human-induced land cover on simulated climates in comparison to having climate-induced land-cover only, since the uncertainties in climate proxy data are large and the land-cover induced differences

470   in climate are small compared to the absolute temperatures and temperature differences due to other forcing (e.g. Strandberg et al., 2011). Moreover, the model-data comparison (Fig. 11; Table 3) is hampered by the irregular spatial distribution of climate proxy data. They do not represent the entire European domain and are often missing in the regions where the largest differences between L and R simulations are suggested by our results. Several sites are located along the coast or in the ocean. Even if we consider only the points in regions where we suspect large differences, such as Scandinavia in winter and western

475   Europe in summer, the conclusion is the same. The climate proxy dataset at hand has not the necessary spatial distribution to assess whether the inclusion of human-induced land cover improves the simulated climate, and whether the RCMs improve simulated regional climate compared to the GCM EC-Earth (Table 3).

480   **Table 3 Correlation (Corr.) and root mean square error (RMSE, °C) between simulated 2.5 ka temperatures and proxy temperatures.**

Climate
of the Past
Discussions

	DJF		JJA	
	Corr.	RMSE	Corr.	RMSE
RCA4-L	0.75	4.05	0.59	4.98
RCA4-R	0.75	4.15	0.6	4.71
HCLIM-L	0.76	3.99	0.61	4.38
HCLIM-R	0.76	3.92	0.6	4.46
EC-Earth	0.74	4.00	0.57	4.41

4.4 Robustness of the results

Even with identical forcing, the response to regional differences in land cover can differ significantly between model
485 simulations. The response in several RCMs (of which RCA4 was one) to idealized land-cover changes was studied for present
climate conditions (Breil et al., 2020; Davin et al., 2020). They showed large agreement across models in the temperature
response to albedo in winter. In summer the analysed RCMs showed different signals in the response to heat flux and
temperature. Russo et al., (2022) suggest that this could be explained by how the land-surface scheme works in the individual
model and how sensitive they are to e.g. perturbations in soil moisture. The small response in latent heat flux and temperature
490 in HCLIM in summer relative to that in RCA4 shows that sensitivity to land-cover changes differs across models, regions and
seasons; however, it is not necessarily a sign of conflict or disagreement between models. Larger land-cover changes may
trigger a similar response in both RCA4 and HCLIM, although testing this would require a series of simulations with
incrementally larger land cover changes, and these tests have not been performed.

The large-scale climate conditions as represented by the driving GCM are important for the RCM simulated regional climate
495 (e.g. Rummukainen, 2010). The dependence of GCM-simulated changes in large-scale circulation on precipitation in the
RCMs is a well-known feature seen in projections of future climate change (e.g. Kjellström et al., 2018; Christensen and
Kjellström, 2020). Also, different GCMs and/or different simulations with the same GCM reflecting natural variability tend
to yield large regional differences (e.g. Deser et al., 2020). For instance, natural variability alone may explain a large part of
differences between models and why one model study differs from another, or from reconstructions using proxy data.
500 Consequently, using other models would have given different results. We acknowledge that we only represent a small part of
the total uncertainty, and that a larger variety of climate models representing natural variability would enable a better
assessment of these differences. Our way of handling model uncertainty is to use two models with different model physics.
As we get the same kind of response as idealised studies of present conditions (Strandberg & Kjellström; Breil et al., 2020;
Davin et al., 2020) and similar studies of past climate (Russo et al., 2022), we can, to some extent, describe the uncertainty
505 associated with responses to land-cover changes due to model physics.

25

Climate of the Past Open Access
Discussions EGU

5 Conclusions

This study describes the climate and land cover 2500 years ago (at 2.5 ka) as simulated by one GCM, two RCMs, one DVM and using one reconstruction of 2.5 ka land cover based on pollen data, statistical interpolation methods and climate model results. The results indicate how climate is influenced by LULCC, and how sensitive RCMs are to differences in land cover.

510   The results presented here suggest that LULCC at 2.5 ka significantly impacted the climate in parts of Europe. Simulations including LULCC give up to 1 °C higher seasonal mean temperature in parts of northern Europe in winter and up to 1.5 °C warmer in southern Europe in summer than simulations with potential land cover. This relatively strong response implies that anthropogenic land-cover changes may have affected the European climate already at 2.5 ka. This also implies that LULCC is important in future scenarios, especially in low-emissions scenarios where the greenhouse gas forcing is relatively small.

515   The models simulate a 2.5 ka climate that was warmer than the PI climate. The largest differences are seen in northern Europe, where the 2.5 ka climate is 2-4 °C warmer than PI. In summer, the difference between the simulated 2.5 ka and PI climates is smaller (0-3 °C), with the smallest differences in southern Europe. Differences in precipitation are mostly within ±10 %. In parts of northern Europe, the climate in 2.5 ka is up to 30 % wetter in winter than that of PI. In summer, there is a tendency for the 2.5 ka climate to be drier than PI in the Mediterranean region.

520   Two different forest types dominate the simulated potential land cover at 2.5 ka: evergreen coniferous forests in northern and eastern Europe, and deciduous broadleaved forests in western Europe. The portion of open land cover is negligible in all forested areas and dominates only in the steppe region of southeast Europe. Reconstructed land cover, however, shows mixed forests in most of Europe. Furthermore, there is a high portion of open land in forested regions, and, besides the steppes, open land cover dominates in most of western and southern Europe. Altogether the reconstructed land cover is considerably more
525   open than the simulated potential land cover in most of Europe.

The choice of land cover has a significant impact on the simulated temperature. Winter and spring temperatures are closely related to albedo, which is largely the same in both RCMs, and is strongly affected by land cover. In summer, the RCMs used in this study respond somewhat differently to land-cover differences, showing that the choice of land cover and model is important for the simulated climate. Summer temperatures are strongly related to differences in heat fluxes between the
530   atmosphere and the ground. Since the response in heat fluxes to differences in land cover depends on model physics, it is more likely that models respond differently in summer than in winter. For summer, RCA4 responds more strongly to the imposed differences in land cover than HCLIM. This explains some differences between the climate conditions simulated by RCA4 and HCLIM. It is difficult to assess which model has the most realistic response. Model performance is dependent on many other factors including, but not limited to, large-scale circulation, parametrisations and resolution. The best way to manage
535   this model uncertainty is to use several models to try to capture the range of possible climates.

The importance of model and land-cover choice calls for caution when designing palaeoclimate experiments. Here we show that it is essential to have a good, well-motivated description of land cover to simulate the same climate with different models in a model ensemble.

Data availability

540   RCM data are available from the Bolin Centre database:
https://doi.org/10.17043/strandberg-2023-bronze-age-1

555   **References**

Aitchison, J.: The Statistical Analysis of Compositional Data. Chapman & Hall, Ltd, London, 1986.

Aitchison, J., 1992, On criteria for measures of compositional differences: Math. Geology, v. 24, p. 365–380.

560   Aitchison, J., Barceló-Vidal, C., Martin-Fernández, J., and Pawlowsky-Glahn, V. (2000). Logratio analysis and compositional
distance. Math. Geol. 32, 271–275. doi: 10.1023/A:1007529726302

Augustin, L., Barbante, C., Barnes, P., et al.: Eight glacial cycles from an Antarctic ice core. Nature 429, 623-628.
https://doi.org/10.1038/nature02599, 2010.
565

Bader, J., Jungclaus, J., Krivova, N., Lorenz, S., Maycock, A., Raddatz, T., Schmidt, H., Toohey, M., Wu, C.-J., and Claussen,
M.: Global temperature modes shed light on the Holocene temperature conundrum. Nat. Commun. 4726, 11. https://
doi.org/10.1038/s41467-020-18478-6, 2020.

570 Belušić, D., Fuentes-Franco, R., Strandberg, G., Jukimenko, A.: Afforestation reduces cyclone intensity and precipitation extremes over Europe. Environ. Res. Lett. 14, https://doi.org/10.1088/1748-9326/ab23b2., 2019.

Belušić, D., de Vries, H., Dobler, A., Landgren, O., Lind, P., Lindstedt, D., Pedersen, R.A., Sánchez-Perrino, J.C., Toivonen, E., van Ulft, B., Wang, F., Andrae, U., Batrak, Y., Kjellström, E., Lenderink, G., Nikulin, G., Pietikäinen, J.-P., Rodríguez-
575 Camino, E., Samuelsson, P., van Meijgaard, E., and Wu, M.: HCLIM38: a flexible regional climate model applicable for different climate zones from coarse to convection-permitting scales, Geosci. Model Dev. 13, 1311-1333. https://doi.org/10.5194/gmd-13-1311-2020., 2020.

Bonferroni, C.E.: Teoria statistica delle classi e calcolo delle probabilità. Pubblicazioni del R Istituto Superiore di Scienze
580 Economiche e Commerciali di Firenze, 1963.

Braconnot, P., Harrison, S., Kageyama, M. et al.: Evaluation of climate models using palaeoclimatic data, Nature Clim Change 2, 417–424, https://doi.org/10.1038/nclimate1456, 2012.

585 Breil, M., Rechid, D., Davin, E.L., de Noblet-Ducoudr e, N., Katragkou, E., Cardoso, R.M., Hoffmann, P., Jach, L.L., Soares, P.M.M., Sofiadis, G., Strada, S., Strandberg, G., Tölle, M.H., and Warrach-Sagi, K. : The opposing effects of re/afforestation on the diurnal temperature cycle at the surface and in the lowest atmospheric model level in the European summer. J. Clim. 33, 21, 9159-9179, https://doi.org/10.1175/JCLI-D-19-0624.1, 2020.

590 Champion T. et al. Prehistoric Europe 1994

Christensen, O.B., and Kjellström, E.: Partitioning uncertainty components of mean climate and climate change in a large ensemble of European regional climate model projections, Clim. Dynam. 54, 4293-4308, https://doi.org/10.1007/s00382-020-05229-y, 2020.
595

Coles J.M. and Harding A.F. The Bronze Age of Europe 1979

Davin, E.L., Rechid, D., Breil, M., Cardoso, R.M., Coppola, E., Hoffmann, P., Jach, L.L., Katragkou, E, De Noblet-Ducoudré, N., Radtke, K., Raffa, M., Soares, P.M.M., Sofiadis, G., Strada, S., Strandberg, G., Tölle, M.H., Warrach-Sagi, K., and
600 Wulfmeyer, V.: Biogeophysical impacts of forestation in Europe: first results from the LUCAS (Land Use and Climate across Scales) regional climate model intercomparison. Earth Syst. Dyn. 11, 183-200, https://doi.org/10.5194/esd-11-183-2020., 2020.

Deser, C., and co-authors: Insights from Earth system model initial-condition large ensembles and future prospects. Nat.
605   Climate Change, 10, 277–286, https://doi.org/10.1038/s41558-020-0731-2, 2020.

Döscher, R., Acosta, M., Alessandri, A., Anthoni, P., Arsouze, T., Bergman, T., Bernardello, R., Boussetta, S., Caron, L.-P.,
Carver, G., Castrillo, M., Catalano, F., Cvijanovic, I., Davini, P., Dekker, E., Doblas-Reyes, F. J., Docquier, D., Echevarria,
P., Fladrich, U., Fuentes-Franco, R., Gröger, M., v. Hardenberg, J., Hieronymus, J., Karami, M. P., Keskinen, J.-P., Koenigk,
610   T., Makkonen, R., Massonnet, F., Ménégoz, M., Miller, P. A., Moreno-Chamarro, E., Nieradzik, L., van Noije, T., Nolan, P.,
O'Donnell, D., Ollinaho, P., van den Oord, G., Ortega, P., Prims, O. T., Ramos, A., Reerink, T., Rousset, C., Ruprich-Robert,
Y., Le Sager, P., Schmith, T., Schrödner, R., Serva, F., Sicardi, V., Sloth Madsen, M., Smith, B., Tian, T., Tourigny, E., Uotila,
P., Vancoppenolle, M., Wang, S., Wårlind, D., Willén, U., Wyser, K., Yang, S., Yepes-Arbós, X., and Zhang, Q.: The EC-
Earth3 Earth system model for the Coupled Model Intercomparison Project 6, Geosci. Model Dev., 15, 2973–3020,
615   https://doi.org/10.5194/gmd-15-2973-2022, 2022.

Field, C. B., Lobell, D. B., Peters, H. A. and Chiariello, N. R.: Feedbacks of terrestrial ecosystems to climate change, Ann Rev
Env Res, 32(1), 1–29, doi:10.1146/annurev.energy.32.053006.141119, 2007.

620   Findell, K. L., Shevliakova, E., Milly, P. C. D. and Stouffer, R. J.: Modeled Impact of Anthropogenic Land Cover Change on
Climate. J Clim 20:3621-3634, 2007.

Gaillard, M.-J., Kleinen, T., Samuelsson, P., Nielsen, A. B., Bergh, J., Kaplan, J. O., Poska, A., Sandström, C., Strandberg,
G., Trondman, A.-K., and Wramneby, A.: Second Assessment of Climate Change for the Baltic Sea Basin, edited by: The
625   BACC II Author Team, Springer International Publishing, Cham, https://doi.org/10.1007/978-3-319-16006-1, 2015.

Gaillard, M.-J., Morrison, K. D., Madella, M., and Whitehouse, N.: Past land-use and land-cover change: the challenge of
quantification at the subcontinental to global scales, PAGES Magazine 26, 3, https://doi.org/10.22498/pages.26.1.3, 2018.

630   Giesecke, T., and Bennett, K.D., 2004. The Holocene spread of Picea abies (L.) Karst. in Fennoscandia and adjacent areas. J.
Biogeogr. 31, 1523e1548.

Giesecke, T., Hickler, T., Kunkel, T., Sykes, M.T., Bradshaw, R.H.W., 2007. Towards an understanding of the Holocene
distribution of Fagus sylvatica L. J. Biogeogr. 34, 118e131.
635

29

Climate
of the Past
Discussions

Open Access

EGU

Giesecke, T. , Brewer, S., Finsinger, W., Leydet, M., Bradshaw, R.H.W. Patterns and dynamics of European vegetation change over the last 15,000 years, Journal of Biogeography, 10.1111/jbi.12974, 44, 7, (1441-1456), (2017).

640 Githumbi, E., Fyfe, R., Gaillard, M.-J., Trondman, A.-K., Mazier, F., Nielsen, A.-B., Poska, A., Sugita, S., Woodbridge, J., Azuara, J., Feurdean, A., Grindean, R., Lebreton, V., Marquer, L., Nebout-Combourieu, N., Stančikaitė, M., Tanţău, I., Tonkov, S., Shumilovskikh, L., and LandClimII data contributors: European pollen-based REVEALS land-cover reconstructions for the Holocene: methodology, mapping and potentials, Earth Syst. Sci. Data, 14, 1581–1619, https://doi.org/10.5194/essd-14-1581-2022, 2022.

645 Jacob, D., Petersen, J., Eggert, B., Alias, A., Christensen, O.B., Bouwer, L.M., Braun, A., Colette, A., Déqué, M., Georgievski, G., Georgopoulou, E., Gobiet, A., Menut, L., Nikulin, G., Haensler, A., Hempelmann, N., Jones, C., Keuler, K., Kovats, S., Kröner, N., Kotlarski, S., Kriegsmann, A., Martin, E., van Meijgaard, E., Moseley, C., Pfeifer, S., Preuschmann, S., Radermacher, C., Radtke, K., Rechid, D., Rounsevell, M., Samuelsson, P., Somot, S., Soussana, J.-F., Teichmann, C., Valentini, R., Vautard, R., Weber, B., and Yiou, P.: EURO-CORDEX: new high-resolution climate change projections for 650 European impact research. Reg. Environ. Change 14 (2), 563-578. 10.1007/s10113-013-0499-2, 2014.

Jia, G., Shevliakova, E., Artaxo, P., De Noblet-Ducoudré, Kitajima, K., Lennard, C., Popp, A., Sirin, A., Sukumar, R., and Verchot, L.: Land-climate interactions. In: Shukla, P.R., Skea, J., Calvo Buendia, E., Masson-Delmotte, Pörtner, H.-O., Roberts, D.C., Zhai, P., Slade, R., Connors, S., van Diemen, R., Ferrat, M., Haughey, E., Luz, S., Neogi, S., Pathak, M., 655 Petzold, J.,
Portugal Pereira, J., Vyas, P., Huntley, E., Kissick, K., Belkacemi, M., Malley, J. (Eds.), Climate Change and Land: an IPCC Special Report on Climate Change, Desertification, Land Degradation, Sustainable Land Management, Food Security, and Greenhouse Gas Fluxes in Terrestrial Ecosystems, 2019.

660 Kageyama, M., Braconnot, P., Harrison, S.P., Haywood, A.M., Jungclaus, J.H., Otto-Bliesner, B.L., Peterschmitt, J.-Y., AbeOuchi, A., Albani, S., Bartlein, P.J., Brierley, C., Crucifix, M., Dolan, A., Fernandez-Donado, L., Fischer, H., Hopcroft, P.O., Ivanovic, R.F., Lambert, F., Lunt, D.J., Mahowald, N.M., Peltier, W.R., Phipps, S.J., Roche, D.M., Schmidt, G.A., Tarasov, L., Valdes, P.J., Zhang, Q., and Zhou, T.: The PMIP4 contribution to CMIP6 - Part 1: overview and overarching analysis plan. Geosci. Model Dev. 11, 1033-1057, https://doi.org/10.5194/gmd-11-1033-2018., 2018.
665

Kaplan, J. O., K. M. Krumhardt, E. C. Ellis, W. F. Ruddiman, C. Lemmen, and K. Goldewijk: Holocene carbon emissions as a result of anthropogenic land cover change, Holocene, 21, 775–792., 2011a

Kaplan, J.O., and Krumhardt, K.M.: The KK10 Anthropogenic Land Cover Change Scenario for the Preindustrial Holocene,
670   Link to Data in NetCDF Format. PANGAEA. https://doi.org/10.1594/PANGAEA.871369, 2011b.

Kaplan, J., Krumhardt, K., Zimmermann, N.: The prehistoric and preindustrial deforestation of Europe. Quat. Sci. Rev. 28,
3016-3034, https://doi.org/10.1016/j.quascirev.2009.09.028., 2009.

675   Kaplan, J.O., Krumhardt, K.M., Ellis, E.C., Ruddiman, W.F., Lemmen, C., and Goldewijk, K.K.: Holocene carbon emissions
as a result of anthropogenic land cover change. Holocene 1-17, https://doi.org/10.1177/0959683610386983., 2010.

Kaplan, J.O., Krumhardt, K.M., Gaillard, M.-J., Sugita, S., Trondman, A.-K., Fyfe, R., Marquer, L., Mazier, F., and Nielsen,
A.B.: Constraining the deforestation history of Europe: evaluation of historical land use scenarios with pollen-based land
680   cover reconstructions. Land 6, 91. https://doi.org/10.3390/land6040091, 2017.

Kaufman, D., McKay, N., Routson, C., et al.: A global database of Holocene paleotemperature records. Scientific Data, 7,
115. doi: 10.1038/s41597-020-0445-3, 2020.

685   Kelliher, F.M., Leuning, R. and Schulze, E.-D.: Evaporation and canopy characteristics ofconiferous
forest and grassland. Oecologia, 95: 153-163, 1993.

Kjellström, E., Brandefelt, J., Näslund, J.-O., Smith, B., Strandberg, G., Voelker, A.H.L., and Wohlfarth, B.: Simulated climate
conditions in Europe during the marine isotope stage 3 stadial. Boreas. https://doi.org/10.1111/j.1502-
690   3885.2010.00143.x.ISSN0300-9483, 2010.

Kjellström, E., Bärring, L., Nikulin, G., Nilsson, C., Persson, N., and Strandberg, G.: Production and use of regional climate
model projections - a Swedish perspective on building climate services. Clim. Serv. 2e3, 15-29,
https://doi.org/10.1016/j.cliser.2016.06.004, 2016.
695
Kjellström, E., Nikulin, G., Strandberg, G., Christensen, O.B., Jacob, D., Keuler, K., Lenderink, G., van Meijgaard, E., Schär,
C., Somot, S., Sørland, S.L., Teichmann, C., and Vautard, R.: European climate change at global mean temperature in-
creases of 1.5 and 2 °C above pre-industrial conditions as simulated by the EURO-CORDEX regional climate models. Earth
Syst. Dynam. 9, 459-478, https://doi.org/10.5194/esd-9-459-2018., 2018.
700

Lehsten, D., Dullinger, S., Huelber, K., Shurgers, G., Cheddadi, R., Laborde, H., Lehsten, V., Francois, L., Dury, M., and Sykes, M.: Modelling the Holocene migrational dynamics of Fagus sylvatica L. and Picea abies (L.). Global Ecology and Biogeography 23(6). p.658-668, 2014.

705 Lehsten, V., Mischurow, M., Lindström, E., Lehsten, D., and Lischke H., LPJ-GM 1.0 : Simulating migration efficiently in a dynamic vegetation model Geoscientific Model Development 12(3). p.893-908, 2019.

Lindgren, F., Rue, H., and Lindström, J.: An explicit link between Gaussian fields and Gaussian Markov random fields: the stochastic partial differential equation approach. J. Roy. Stat. Soc. B Stat. Methodol. 73 (4), 423-498. https://doi.org/
710 10.1111/j.1467-9868.2011.00777.x, 2011.

Lindgren, A., Lu, Z., Zhang, Q., & Hugelius, G. (2021). Reconstructing past global vegetation with random forest machine learning, sacrificing the dynamic response for robust results. Journal of Advances in Modeling Earth Systems, 13(2), e2020MS002200.
715

Manabe, S., & Wetherald, R. T. (1967). Thermal equilibrium of the atmosphere with a given distribution of relative humidity. Journal of the Atmospheric Sciences, 24(3), 241–259. https://doi.org/10.1175/1520-0469(1967)024<0241:TEOTAW>2.0.CO;2

720 Miller, P.A., Giesecke, T., Hickler, T., Bradshaw, R.H.W., Smith, B., Seppä, H., Valdes, P.J., Sykes, M.T., 2008. Exploring climatic and biotic controls on Holocene vegetation change in Fennoscandia. J. Ecol. 96, 247e259.

Otto-Bliesner, B.L., Braconnot, P., Harrison, S.P., Lunt, D.J., Abe-Ouchi, A., Albani, S., Bartlein, P.J., Capron, E., Carlson, A.E., Dutton, A., Fischer, H., Goelzer, H., Govin, A., Haywood, A., Joos, F., LeGrande, A.N., Lipscomb, W.H., Lohmann,
725 G., Mahowald, N., Nehrbass-Ahles, C., Pausata, F.S.R., Peterschmitt, J.Y., Phipps, S.J., Renssen, H., and Zhang, Q.: The PMIP4 contribution to CMIP6 - Part 2: two interglacials, scientific objective and experimental design for Holocene and Last Interglacial simulations. Geosci. Model Dev. 10, 3979e4003. https://doi.org/10.5194/gmd-10-3979-2017, 2017.

Pinke, Z., Ferenczi, L., Romhányi, B. F., Gyulai, F., Laszlovszky, J., Mravcsik, Z., … Gábris, G. (2017). Zonal assessment of
730 environmental driven settlement abandonment in the Trans-Tisza region (Central Europe) during the early phase of the Little Ice Age. Quaternary Science Reviews, 157, 98–113. https://doi.org/10.1016/J.QUASCIREV.2016.12.010

Pirzamanbein, B., Lindström, J., Poska, A., and Gaillard, M.-J.: Modelling spatial compositional data: reconstructions of past land cover and uncertainties. Spat. Stat. 24, 14e31. https://doi.org/10.1016/j.spasta.2018.03.005., 2018.

735

Pirzamanbein, B., Poska, A., and Lindström, J.: Bayesian reconstruction of past land cover from pollen data: model robustness and sensitivity to auxiliary variables. Earth Space Sci. 7, 1. https://doi.org/10.1029/2018EA000547, 2020.

Ruddiman, W. F.: The anthropogenic greenhouse era began thousands of years ago, Clim Change, 61, 261–293, 2003.

740

Ruddiman, W.F., Fuller, D.Q., Kutzbach, J.E., Tzedakis, P.C., Kaplan, J.O., Ellis, E.C., Vavrus, S.J., Roberts, C.N., Fyfe, R., He, F. and Lemmen, C.: Late Holocene climate: Natural or anthropogenic? Rev. Geophysics, 54, 93-118, 2016..

Ruddiman, W.F., Kutzbach, J.E. and Vavrus, S.J.: Can natural or anthropogenic explanations of late-Holocene CO2 and CH4

745 increases be falsified? The Holocene, 21, 865-8879, 2011.

Rummukainen, M.: State-of-the-art with regional climate models, WIREs Clim. Change, 1, 82–96, 2010.

Russo, E., Fallah, B., Ludwig, P., Karremann, M., and Raible, C. C.: The long-standing dilemma of European summer

750 temperatures at the mid-Holocene and other considerations on learning from the past for the future using a regional climate model, Clim. Past, 18, 895–909, https://doi.org/10.5194/cp-18-895-2022, 2022.

Sitch, S., Smith, B., Prentice, I.C., Arneth, A., Bondeau, A., Cramer, W., Kaplan, J.O., Levis, S., Lucht, W., Sykes, M.T., Thonicke, K., and Vevensky, S.: Evaluation of ecosystem dynamics, plant geography and terrestrial carbon cycling in the LPJ

755 dynamic global vegetation model. Global Change Biol. 9, 161-185. https://doi.org/10.1046/j.1365-2486.2003.00569.x, 2003.

Smith, B., Prentice, I.C., and Sykes, M.T.: Representation of vegetation dynamics in the modelling of terrestrial ecosystems: comparing two contrasting approaches within European climate space. Global Ecol. Biogeogr. 10, 621-637. https://doi.org/10.1046/j.1466-822X.2001.t01-1-00256.x, 2001.

760

Smith, B., Wårlind, D., Arneth, A., Hickler, T., Leadley, P., Siltberg, J., and Zaehle, S.: Implications of incorporating N cycling and N limitations on primary production in an individual-based dynamic vegetation model. Biogeosciences 11, 2027e2054. https://doi.org/10.5194/bg-11-2027-2014, 2014.

765 Sørland, S.L., Schär, C., Lüthi, D., and Kjellström, E.: Bias patterns and climate change signals in GCM-RCM model chains. Environ. Res. Lett. 13, 074017, https://doi.org/10.1088/1748-9326/aacc7, 2018.

Stadelmaier, K.H., Ludwig, P., Bertran, P., Antoine, P., Shi, X., Lohmann, G., and Pinto, J.G.: A new perspective on permafrost boundaries in France during the Last Glacial Maximum, Clim. Past 17, 2559-2576. https://doi.org/10.5194/cp-17-2559-2021., 2021.

Stocker, B.D., Strassmann, K. and Joos, F.: Sensitivity of Holocene atmospheric CO 2 and the modern carbon budget to early human land use: analyses with a process-based model. Biogeosciences, 8, 69-88, 2011.

Strandberg, G., and Kjellström, E.: Climate impacts from afforestation and deforestation in Europe. Earth Interact. 23, 1e27. https://doi.org/10.1175/EI-D-17-0033.1., 2019.

Strandberg, G., Kjellström, E., Poska, A., Wagner, S., Gaillard, M.-J., Trondman, A.-K., Mauri, A., Davis, B.A.S., Kaplan, J.O., Birks, H.J.B., Bjune, A.E., Fyfe, R., Giesecke, T., Kalnina, L., Kangur, M., van der Knaap, W.O., Kokfelt, U., Kuneš, P., Latalowa, M., Marquer, L., Mazier, F., Nielsen, A.B., Smith, B., Seppä, H., and Sugita, S.: Regional climate model simulations for Europe at 6 and 0.2 k BP: sensitivity to changes in anthropogenic deforestation, Clim. Past 10, 661-680, https://doi.org/10.5194/cp-10-661-2014., 2014.

Strandberg, G., Bärring, L., Hansson, U., Jansson, C., Jones, C., Kjellström, E., Kolax, M., Kupiainen, M., Nikulin, G., Samuelsson, P., Ullerstig, A., and Wang, S.: CORDEX scenarios for Europe from the Rossby Centre regional climate model RCA4, SMHI Meteorol. Climatol. Rep. 116, 84. Norrköping. https://www.smhi.se/polopoly_fs/1.90275!/Menu/general/extGroup/attachmentColHold/mainCol1/file/RMK_116.pdf, 2015.

Strandberg, G., Lindström, J., Poska, A., Zhang, Q., Fyfe, R., Githumbi, E., Kjellström, E., Mazier, F., Nielsen, A. B., Sugita, S., Trondman, A.-K., Woodbridge, J., and Gaillard, M.-J.: Mid-Holocene European climate revisited: New high-resolution regional climate model simulations using pollen-based land-cover, Quaternary Science Reviews, https://doi.org/10.1016/j.quascirev.2022.107431., 2022.

Sugita, S.: Theory of quantitative reconstruction of vegetation I: pollen from large sites REVEALS regional vegetation composition, Holocene 17 (2), 229-241, https://doi.org/10.1177/0959683607075837, 2007.

Trondman, A.-K., Gaillard, M.-J., Mazier, F., Sugita, S., Fyfe, R.M., Nielsen, A.B., Twiddle, C., Barratt, P., Birks, H.J.B., Bjune, A.E., Bj€orkman, L., Broström, A., Caseldine, C.J., David, R., Dodson, J., Dörfler, W., Fischer, E., van Geel, B., Giesecke, T., Hultberg, T., Kalnina, L., Kangur, M., van der Knaap, P.W.O., Koff, T., Kunes, P., Lageras, P., Latalowa, M., Lechterbeck, J., Leroyer, C., Leydet, M., Lindbladh, M., Marquer, L., Mitchell, F.J.G., Odgaard, B.V., Peglar, S.M., Persson,

T., Poska, A., Rösch, M., Seppä, H., Veski, S., and Wick, L.: Pollen-based quantitative reconstructions of Holocene regional vegetation cover (plant-functional types and land-cover types) in Europe suitable for climate modelling. Global Change Biol. 21 (2), 676-697. https://doi.org/10.1111/gcb.12737, 2015.

805 van Vuuren, D.P., Edmonds, J., Kainuma, M. et al.: The representative concentration pathways: an overview. Climatic Change 109, 5, https://doi.org/10.1007/s10584-011-0148-z, 2011.

Velasquez, P., Kaplan, J.O., Messmer, M., Ludwig, P., and Raible, C.C.: The role of land cover in the climate of glacial Europe. Clim. Past 17, 1161e1180. https://doi.org/10.5194/cp-17-1161-2021, 2021.

810

Zhang, Q., Berntell, E., Axelsson, J., Chen, J., Han, Z., de Nooijer, W., Lu, Z., Li, Q., Zhang, Q., Wyser, K., and Yang, S.: Simulating the mid-Holocene, last inter-glacial and mid-Pliocene climate with EC-Earth3-LR, Geosci. Model Dev 14, 1147e1169. https://doi.org/10.5194/gmd-14-1147-2021, 2021.

815

820

825

830

Appendix A

Table A1 Groups of land-cover types used in this study. Ericaceae*(MTSE): the pollen productivity used for Ericaceae pollen in the REVEALS reconstruction represents the mean pollen productivity of several species of which Arbutus unedo, Erica arborea, E. cinerea and E. multiflora are dominant. The genus Calluna vulgaris (heather, LSE) also belongs to the Ericaceae family but its pollen productivity has been estimated separately (Githumbi et al., 2021). Cerealia t.: all cereals except Secale cereale (rye) that is easily that is easily separated on the basis of pollen morphology and for which pollen productivity was estimated separately. Abbreviation: t = type. of land-cover types (LCTs) and Plant Functionnal Types (PFTs) used in this study. **The most recent plant taxonomy has merged the family Chenopodiaceae into the family Amaranthaceae, i.e. "new" Amaranthaceae = "former" Amaranthaceae + Chenopodiaceae. Pollen analysts have mostly used the name Chenopodiaceae for this pollen-morphological type, but it includes all species from the two former families, therefore the name Amaranthaceae/Chenopodiaceae.

Land-cover types (LCTs)	PFT	PFT definition	Plant taxa/Pollen-morphological types
	TBE1	Shade-tolerant evergreen trees	*Picea abies* (Norway spruce)
	TBE2	Shade-tolerant evergreen trees	*Abies alba* (Silver fir)
	IBE	Shade-intolerant evergreen trees	*Pinus sylvestris* (Scots pine)
	MTBE	Mediterranean shade-tolerant broadleaved evergreen trees	*Phillyrea* (mock privet)
Evergreen trees and shrubs (ET)			*Pistacia* (lentisk, mastic)
			Quercus evergreen t. (evergreen oak species)
	TSE	Tall shrub, evergreen	*Juniperus communis* (common juniper)
	MTSE	Mediterranean broadleaved tall shrubs, evergreen	*Ericaceae** (heather family)
			Buxus sempervirens (common box)
Summer-green trees and shrubs (ST)	IBS	Shade-intolerant summer-green trees	*Alnus glutinosa* (common alder)
			Betula (birch species)

Climate
of the Past
Discussions

			Carpinus betulus (common hornbeam)
			Carpinus orientalis (oriental hornbeam)
			Castanea sativa (sweet chestnut)
	TBS	Shade-tolerant summer-green trees	*Corylus avellana* (common hazel)
			Fagus sylvatica (European beech)
			Fraxinus (ash species)
			Quercus deciduous t. (summer-green oak species)
			Tilia (linden species)
			Ulmus (elm species)
	TSD	Tall shrub, summer-green	*Salix* (willow species (osier, sallow))
	LSE	Low shrub, broadleaved evergreen	*Calluna vulgaris* (heather)
Open land (OL)	GL	Grassland - all herbs	*Artemisia* (mugwort species)
			Amaranthaceae/ Chenopodiaceae (amaranth family/e.g. goosefoot**)
			Cyperaceae (sedges)
			Filipendula (meadowseet)
			Poaceae (grass family)

Climate
of the Past
Discussions

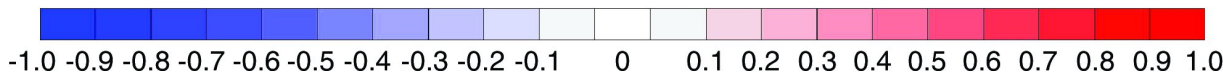|		*Plantago lanceolata* (ribwort plantain)
		Rumex acetosa-t (common sorrel and some other Rumex (dock) species)
AL	Agricultural land - cereals	*Cerealia-t* (all cereals except *Secale cereale* (rye))
		Secale cereale (rye)

Climate
of the Past
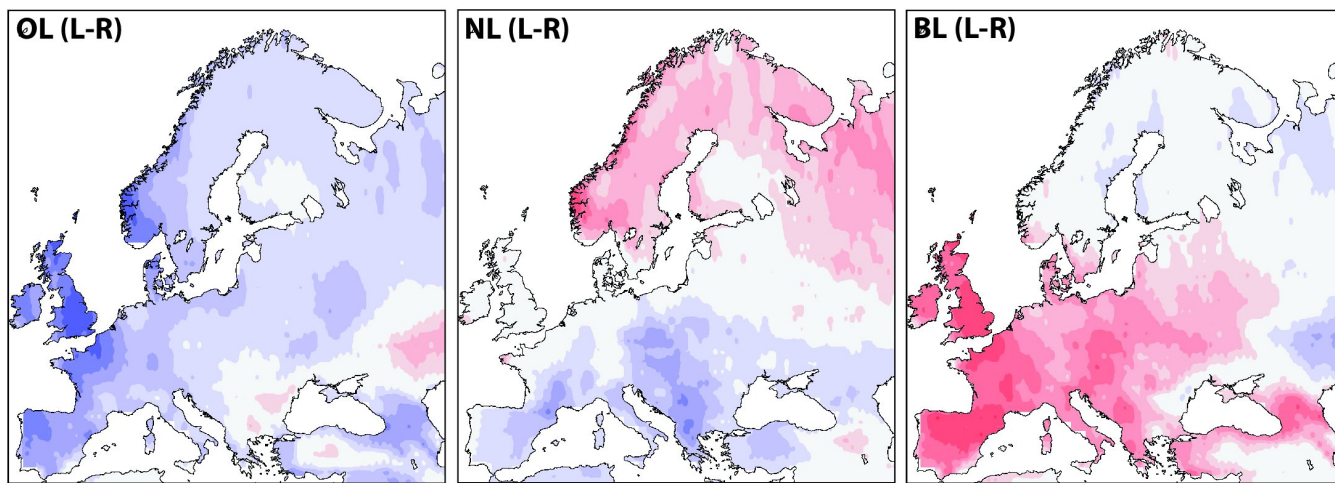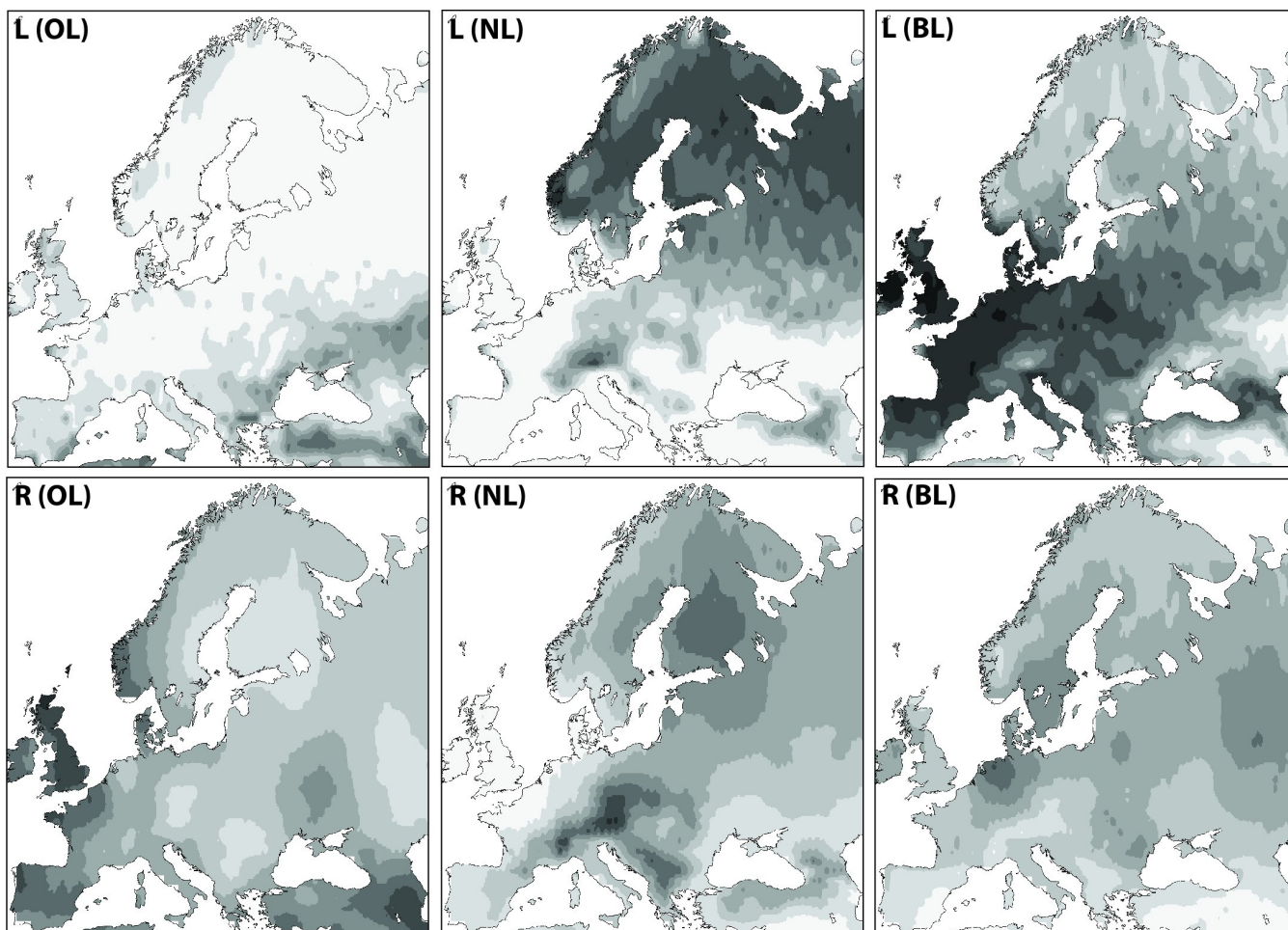Discussions

Open Access

EGU

Fig A1 Upper panels: Cover (in fraction of grid cell) of open land (OL), evergreen trees (ET), and summer-green trees (ST) at 2.5 ka in Europe as, first row: simulated by LPJ-GUESS using climate input from EC-Earth (L), and second row: estimated using pollen data and the REVEALS model (R). Lower panels: Difference between L and R cover (R-L). See main text under methods and results for details.

840